IEEE Access
Multidisciplinary | Rapid Review | Open Access Journal

Received 15 May 2023, accepted 26 May 2023, date of publication 31 May 2023, date of current version 9 June 2023.

Digital Object Identifier 10.1109/ACCESS.2023.3281758

RESEARCH ARTICLE

Center-of-Rotation-Augmented Kalman Filter for Adaptive Attitude Reference System

MIN SEOK LEE[1], (Graduate Student Member, IEEE), JUNGMIN PARK[2], AND CHAN GOOK PARK[3], (Member, IEEE)

[1]Department of Aerospace Engineering, Automation and System Research Institute, Seoul National University, Seoul 08826, South Korea
[2]Agency for Defense Development, Daejeon 34060, South Korea
[3]Department of Aerospace Engineering, Institute of Advanced Aerospace Technology, Seoul National University, Seoul 08826, South Korea

Corresponding author: Chan Gook Park (chanpark@snu.ac.kr)

This work was supported by the National Research Foundation of Korea (NRF) funded by the Ministry of Science and Information and Communications Technology (ICT), Republic of Korea, under Grant NRF-2022R1A2 C2012166.

ABSTRACT This paper proposes a novel augmented Kalman filter-based attitude reference system (ARS) that uses an inertial sensor comprised of a tri-axial gyroscope and a tri-axial accelerometer. For accurate estimation of attitude using an inertial sensor, effective compensation of the non-gravitational acceleration is crucial. The proposed method resolves this issue by using a novel rotational motion detector to adaptively eliminate non-gravitational acceleration. The types of motions that the system experiences are accurately distinguished by augmenting center of rotation to the state vector. Due to our unconventional augmented state vector, the reformed filter properties have been thoroughly examined, and an observability analysis has been carried out. An extensive experimental validation was conducted under six diversified scenarios from the author-collected and open-source datasets, including both rotation-only and translation-rotation-combined motions. The results demonstrate that the proposed method accurately estimates attitude with sub-degree errors for most trials, proving robustness and accuracy under various motions. A comparative analysis reveals that our method outperforms the conventional method and the MTx algorithm.

INDEX TERMS Accelerometer, attitude reference system, center of rotation, gyroscope, inertial measurement units, Kalman filter.

I. INTRODUCTION

Since the development of Micro Electro-Mechanical Systems (MEMS) technology, inertial measurement units (IMUs) has been widely utilized on various applications, including indoor navigation [1], motion capture [2], unmanned aerial vehicles (UAVs) [3], and many more. Thanks to their small-sized, low-cost, and low power consuming nature, IMUs have very little restrictions on which platform they are mounted on, namely smartphones, quadrotors, and wearable devices. Using measurements from the gyroscope, the inertial navigation system (INS) algorithm can deliver orientation (roll, pitch, and yaw) through integrating angular rates, when initial angles are known. However, gyroscopes are vulnerable to a drift which rapidly increases over time. Hence, to achieve long-term stability and accuracy, other sensors are often used together. The most common one is the accelerometer, which outputs specific force. When stationary, the accelerometer can be used to estimate gravity vector, and thus provide attitude (roll and pitch) information of the platform. A system which fuses measurements from gyroscope and accelerometer to estimated attitude is called Attitude Reference System (ARS). When outputs from magnetometer is combined with ARS, the system is now able to estimate heading (yaw), hence called Attitude and Heading Reference System (AHRS). Though the scope of this paper is ARS, previous works we cover in this paper are not limited to ARS, since many works of AHRS still propose methods to deals with acceleration.

A. RELATED WORK

Plentiful works have addressed the means of sensor fusion with respect to ARS and AHRS. The most common

The associate editor coordinating the review of this manuscript and approving it for publication was Angel F. García-Fernández.

approaches, by far, are complementary filter [4], [5], [6], [7], [8], [9], [10] and Kalman filter or its variants [1], [11], [12], [13], [14], [15], [16], [17], [18], [19], [20], [21], [22], [23], [24], [25], [26], [27], [28], [29]. Complementary filter is a simple data fusion technique which combines complementary information from two different sensors in the frequency domain. Reference [4] showed that the gyroscope and accelerometer to have complementary frequency response, making them suitable candidates for complementary filter. Generally, gyroscopes and accelerometers are passed through a high-pass filter and a low-pass filter, respectively, as the former experience a drift in the low-frequency domain, and the latter are susceptible to noises of high-frequency domain. Mahony [5] proposed a design of nonlinear complementary filter on special orthogonal group. Madgwick [30] adopted Gradient Descent Algorithm (GDA) to estimate orientation in a computationally efficient manner. More recently, Liu and Zhu [6] proposed an attitude estimation algorithm of multi-sample equivalent rotation vector using angular rates rather than angular increments. Wu [7] contributed with a quaternion-based fast complementary filter (FCF) that has much less convergence time than the previous works. Despite many advantages including efficiency, above works of complementary filter still suffer from lack of adaptability as their parameters, namely gains, are usually fixed and performance deteriorates quickly when circumstances regarding motions change. To resort to a more robust fusion technique, our proposed method is based on Kalman filter.

When the outputs of gyroscope and accelerometer are fused together, it is imperative to correctly estimate the gravity vector from the accelerometer measurements. Ideally, the system should experience little to no acceleration compared to accelerometer noise to achieve so. However, handheld devices such as smartphones and smartwatches are subject to dynamic motions, making it difficult for accelerometer to estimate a pure gravity vector. To deal with such non-gravitational acceleration, or external acceleration, numerous approaches have been proposed, and most can be categorized into two: adaptation [1], [10], [14], [15], [16], [17], [18], [19], [20], [21], [22], [23], [31], [32] and modelling [3], [24], [25], [26], [27], [28], [29], [33]. Works that adopt adaptation methods usually distinguishes motion as static and dynamic, and adapts accordingly. Li and Wang [14] proposed a Kalman filter-based AHRS that adaptively tunes the measurement noise covariance depending on three different scenarios of non-acceleration, low-acceleration, and high-acceleration modes. Munguía and Grau [15] presented an extended Kalman filter-based (EKF) AHRS in a quaternion form that detects static mode with the well-known Stance Hypothesis Optimal Detector (SHOE) [34]. Makni [1] proposed an energy-efficient quaternion-based adaptive Kalman filter with a hybrid detector that completely switches off the gyroscope when static. Tong [16] implemented a hidden Markov Model (HMM) recognizer to a multiplicative extended Kalman filter (MEKF) to adaptively tune noise covariance depending on disturbance caused by motion. While stated works show satisfactory results, using adaptation method alone will result in large attitude error when the system is under dynamic situation for an extended period of time. Furthermore, information on the nature of the motion are not fully exploited, since modelling of the non-gravitational acceleration and/or the kinematics itself is absent.

Dealing with external acceleration through modelling is also a frequently used method in the field of ARS/AHRS. Lee [24] proposed a Kalman filter-based ARS that models the external acceleration as a first-order low-pass filtered white noise process. Though such modelling approach is adopted by several works that followed [11], [25], [26], yet, the model is not based on the actual nature of the non-gravitational acceleration, lacking justification behind the approach. [27] adopts the model of [24] and employs an augmented Kalman filter to describe the dynamics, similar to our proposed work. However, [27] is limited to a ball-and-socket joint application, contrary to our work which can be applied to complex motions with varying center of rotation. Kim [3] studied attitude estimation on a small aerial vehicle, where the external acceleration has certain frequency profile as it is induced by the platform vibration of the actuators, and hence implemented second-order infinite impulse response (IIR) notch filter. Maliňák [28] proposed an EKF-based AHRS with a newly developed concept of synthetic acceleration that models the non-gravitational acceleration differently depending on whether the dynamics of the body is in a nominal or a rare-normal situation. Park [29] presented an indirect Kalman filter-based AHRS where the measurement noise covariance was modelled using ellipsoidal method, rather than modelling the external acceleration itself. Takeda [35] estimated attitude by placing inertial sensors on specific points on limb segments, modelling human gait as a series of rigid body rotation. However, such modelling demanded many parameters that must be measured prior to motion. Although numerous attempts have been made to accurately model the acceleration or the kinematics, the results are still unsatisfactory. The models are either unrealistic with no basis on the actual dynamics, too tailored to a specific application, or in need of predetermined parameters.

B. MOTIVATION AND CONTRIBUTION

After surveying on existing attitude estimating methods, we have gathered a few insights and motivations towards developing our novel method proposed in this paper. First, sensor fusion technique combining outputs of gyroscope and accelerometer that enables robust estimation of attitude is in need. Second, a system should deliver excellent performance under changing circumstances through an adaptation method that withstands dynamic motions with severe acceleration for a prolonged time. Third, appropriate modelling of the kinematics should be in place to not only facilitate a more accurate attitude estimation but also improve versatility of the system regarding various scenarios and platforms ARS may

be utilized. When doing so, using predetermined parameters should be shunned.

Hence, in this paper we present a novel indirect Kalman filter-based ARS that estimates attitude and gyro bias along with center of rotation. The state vector of the filter is augmented to include center of rotation, which not only improves accuracy of attitude estimation but also robustness towards various types of dynamic not limited to rotation-only or translation-only motions. To adaptively cope with changing dynamics, a rotational motion detector is developed to efficiently equip our system with appropriate measurement model consistent with current dynamics. The structure of the filter is thoroughly explained, with a detailed derivation of newly devised measurement noise covariance matrix and an observability analysis. The performance of the proposed ARS is verified experimentally against the MTx algorithm by Xsens and a conventional method based on the work of Li and Wang [14]. The tested scenarios consist of six cases, four of which are from the author-collected dataset and the rest from the open-source dataset Berlin Robust Orientation Estimation Assessment Dataset (BROAD) [36]. To highlight the accuracy and robustness of our proposed algorithm, the tested datasets are comprised of differing values of accelerations, centers of rotation, and types of motion, including rotation-only and rotation-translation-combined motions

The main contributions of this paper are restated as follows:

1) An indirect Kalman filter-based ARS estimating center of rotation online is proposed. Estimation of the rotational arm improves accuracy as well as the versatility of our system.
2) A rotational motion detector is proposed to robustly adapt to ever-changing dynamics with a corresponding measurement model and a noise covariance.
3) The unconventional measurement noise covariance matrix pertinent to the proposed system is meticulously derived.

The paper is organized as follows. In Section II, we give a simple formulation of the Kalman filter-based Attitude Reference System, and a brief summary of previous methods that deal with external acceleration. In Section III, we propose a novel indirect Kalman filter-based ARS, with a rotational motion detector, that estimates center of rotation online. In Section IV, we evaluate the performance of the proposed method by comparing with conventional methods against several different scenarios, including highly challenging motions. The paper concludes with Section V. Notations used throughout this paper is presented in Table 1. Less frequently used notations and abbreviations are defined separately when they first appear in this paper.

TABLE 1. Notations.

Frames	
b	Body frame
n	Local navigation frame
N, E, D	North, East, Down of the navigation frame
Kinematic quantities	
γ, θ, ψ	Roll, Pitch, Yaw
$\boldsymbol{\phi}$	$[\gamma \quad \theta \quad \psi]^T$
$\mathbf{C}_b^n$	Direction Cosine Matrix (DCM, body frame to local navigation frame)
g	Gravitational acceleration
r	Center of rotation ($\lvert\mathbf{r}^b\rvert$)
Sensor-related quantities	
$\mathbf{f}$	Accelerometer measurement
$\boldsymbol{\omega}$	Gyroscope measurement
Δt	Sampling time
b_g	Gyroscope bias
Kalman filter quantities	
$\mathbf{x}$	State vector
$\boldsymbol{\Phi}$	System matrix (continuous)
$\mathbf{F}$	System matrix (discrete)
$\mathbf{w}$	Process noise ($\mathbf{w} \sim N(0, \mathbf{Q})$)
$\mathbf{z}$	Measurement
$\mathbf{H}$	Observation matrix
$\mathbf{v}$	Measurement noise ($\mathbf{v} \sim N(0, \mathbf{R})$)
$\mathbf{K}$	Kalman gain
$\mathbf{P}$	Error covariance matrix
$\mathbf{Q}$	Process noise covariance matrix
$\mathbf{R}$	Measurement noise covariance matrix
$(\cdot)^+$	*Posteriori* value
$(\cdot)^-$	*Priori* value
Others	
$\mathbf{I}_{n\times n}$	n-by-n Identity matrix
$\mathbf{0}_{m\times n}$	m-by-n Zeros matrix
$[(\cdot)\times]$	Skew-symmetric matrix
$\widehat{(\cdot)}$	Estimate value of $(\cdot)$
$\widetilde{(\cdot)}$	Measured value of $(\cdot)$
$\delta(\cdot)$	Error of $(\cdot)$
$\mathbf{d}$	External acceleration
$\mathrm{E}[\cdot]$	Expectation of $(\cdot)$
$\lvert\cdot\rvert$	Norm of $(\cdot)$
PSD	Power Spectral Density

II. KALMAN FILTER-BASED ARS

An ARS usually employs the Kalman filter for the fusion of gyro and accelerometer information. The relationship between attitude and accelerometer measurements when the sensor is static is as follows.

$$\gamma = \arctan\left(\frac{f_y}{f_z}\right) \tag{1}$$

$$\theta = \arctan\left(\frac{f_x}{\sqrt{f_y^2 + f_z^2}}\right) \tag{2}$$

The nominal state vector $\mathbf{x}$ is defined as

$$\mathbf{x} = \begin{bmatrix} \gamma & \theta & | & b_{g,x} & b_{g,y} & b_{g,z} \end{bmatrix}^T \tag{3}$$

where $b_{g,x}$, $b_{g,y}$, and $b_{g,z}$ are the gyro bias in the x-, y-, and z-axes, respectively. The error state vector $\delta\mathbf{x}$ is defined as

$$\delta\mathbf{x} = \begin{bmatrix} \varphi_N & \varphi_E & | & \delta b_{g,x} & \delta b_{g,y} & \delta b_{g,z} \end{bmatrix}^T \tag{4}$$

where $\boldsymbol{\varphi} = \begin{bmatrix} \varphi_N & \varphi_E & \varphi_D \end{bmatrix}^T$ is known as the Psi-angle error, used by numerous previous works including [14], representing the difference between the true navigation frame and the computed navigation frame.

$\mathbf{C}_b^n$ is expressed in terms of Euler angles as follows.

$$\mathbf{C}_b^n = \begin{bmatrix} c\psi c\theta & c\psi s\theta s\gamma - s\psi c\gamma & c\psi s\theta c\gamma + s\psi s\gamma \\ s\psi c\theta & s\psi s\theta s\gamma + c\psi c\gamma & s\psi s\theta c\gamma - c\psi s\gamma \\ -s\theta & c\theta s\gamma & c\theta c\gamma \end{bmatrix} \tag{5}$$

The small case letters "c" and "s" stand for "cosine" and "sine", respectively. The relationship between the Euler angle error and the Psi-angle error is defined as follows.

$$\begin{aligned} \begin{bmatrix} \varphi_N \\ \varphi_E \end{bmatrix} &= \begin{bmatrix} c\psi & -s\psi \\ s\psi & c\psi \end{bmatrix} \left(\begin{bmatrix} c\theta & 0 \\ 0 & 1 \end{bmatrix} \begin{bmatrix} \delta\gamma \\ 0 \end{bmatrix} + \begin{bmatrix} 0 \\ \delta\theta \end{bmatrix} \right) \\ &= \begin{bmatrix} c\theta c\psi & -s\psi \\ c\theta s\psi & c\psi \end{bmatrix} \begin{bmatrix} \delta\gamma \\ \delta\theta \end{bmatrix} \end{aligned} \tag{6}$$

The Euler angle errors shown in above equation are defined as follows.

$$\begin{aligned} \delta\gamma &= \gamma - \hat{\gamma} \\ \delta\theta &= \theta - \hat{\theta} \end{aligned} \tag{7}$$

As for the gyro bias, the relationship between the nominal value and the error is as follows.

$$\delta\boldsymbol{b}_g = \boldsymbol{b}_g - \hat{\boldsymbol{b}}_g \tag{8}$$

The indirect Kalman filter corrects the nominal state $\mathbf{x}$ with the error state $\delta\mathbf{x}$ using equations (7) and (8).

In the absence of external acceleration, the nonlinear continuous system and measurement models adopted from [37] are as follows.

System model (nonlinear, continuous):

$$\begin{aligned} \dot{\gamma} &= \omega_x + \omega_y\,(s\gamma t\theta) + \omega_z\,(c\gamma t\theta) + b_{g,x} + b_{g,y}\,(s\gamma t\theta) \\ &\quad + b_{g,z}\,(c\gamma t\theta) + \mathrm{w}_x + \mathrm{w}_y\,(s\gamma t\theta) + \mathrm{w}_z\,(c\gamma t\theta) \\ \dot{\theta} &= \omega_y c\gamma - \omega_z s\gamma + \mathrm{w}_y c\gamma + b_{g,y} c\gamma - \mathrm{w}_z s\gamma - b_{g,z} s\gamma \\ \dot{\boldsymbol{b}}_g &= \mathbf{w}_g \end{aligned} \tag{9}$$

where the small case letter "t" stands for "tangent".

Measurement model (nonlinear, continuous):

$$\begin{aligned} \mathbf{z} = \tilde{\mathbf{f}}^{\mathrm{b}} &= \mathbf{C}_n^b \begin{bmatrix} 0 & 0 & -g \end{bmatrix}^T + \mathbf{v} \\ &= \hat{\mathbf{C}}_n^b \left(\mathbf{I} - [\boldsymbol{\varphi}\times]\right) \begin{bmatrix} 0 & 0 & -g \end{bmatrix}^T + \mathbf{v} \end{aligned} \tag{10}$$

The relationship between $\hat{\mathbf{C}}_n^b$ and $\mathbf{C}_n^b$ is adopted from [38], which also provides a detailed derivation.

From above models, the linearized discrete error state models can be shown as follows.

System model (linear, discrete):

$$\delta\mathbf{x}_k = \boldsymbol{\Phi}_{k-1}\delta\mathbf{x}_{k-1} + \mathbf{w}_{k-1} \tag{11}$$

$$\boldsymbol{\Phi}_k = \mathbf{I}_{5\times5} + \mathbf{F}_k\Delta t, \quad \mathbf{F}_k = \begin{bmatrix} \mathbf{0}_{2\times2} & \mathbf{C}_{1,2r} \\ \mathbf{0}_{3\times2} & \mathbf{0}_{3\times3} \end{bmatrix} \tag{12}$$

where $\mathbf{C}_{1,2r}$ is the first two rows of $\hat{\mathbf{C}}_b^n$. The discretization method of $\boldsymbol{\Phi}$ is explained in Section III-B.

Measurement model (linearized, discrete):

$$\delta\mathbf{z}_k = \tilde{\mathbf{f}}_k + \hat{\mathbf{C}}_n^b \begin{bmatrix} 0 & 0 & g \end{bmatrix}^T = \mathbf{H}_k\delta\mathbf{x}_k + \mathbf{v}_k \tag{13}$$

$$\mathbf{H}_k = \begin{bmatrix} \mathbf{C}_{1,2c} & \mathbf{0}_{3\times3} \end{bmatrix} \tag{14}$$

where $\mathbf{C}_{1,2c}$ is the first two columns of $\hat{\mathbf{C}}_n^b[\mathbf{g}\times]$, $\delta\mathbf{z}_k$ is the measurement residual, and $\tilde{\mathbf{f}}_k$ is the measurement specific force.

However, in the presence of dynamic motion, the accelerometer measurements also measure non-gravitational acceleration, and hence the force measurement equation is as follows.

$$\tilde{\mathbf{f}}_k = \mathbf{C}_n^b \begin{bmatrix} 0 & 0 & -g \end{bmatrix}^T + \mathbf{d}_k \tag{15}$$

Note here that the measurement noise $\mathbf{v}_k$ is incorporated in external acceleration $\mathbf{d}_k$. To deal with such external acceleration, previous studies adopt methods such as adaptation and modeling, as mentioned in Section I-A.

III. PROPOSED CENTER-OF-ROTATION BASED ARS

This section presents the proposed center-of-rotation based ARS that uses a rotational motion detector to estimate attitude, gyro bias, and center of rotation. The structure of our indirect Kalman filter-based system and a detailed derivation of the measurement noise covariance matrix are also described in depth.

A. SYSTEM OVERVIEW

The structure of the proposed algorithm is illustrated as a schematic block diagram in Fig. 1. The system is based on the indirect Kalman filter, where accelerometer measurements with the *priori* values from time propagation go through our rotational motion detector. Depending on which step of the detector the system is determined to be dynamic, the filter adaptively adopts specific measurement model and noise covariance apt for each circumstance. The details of the adaptive algorithm are explained thoroughly in the following subsection.

B. PROPOSED SYSTEM DESCRIPTION

We propose a kinematic modelling method where the model parameter, center of rotation, is estimated online. The parameters to be estimated are the x, y, and z positions of center of rotation in the sensor frame. The center of rotation vector with respect to sensor frame is denoted as $\mathbf{r}^{\mathrm{b}}$, while its

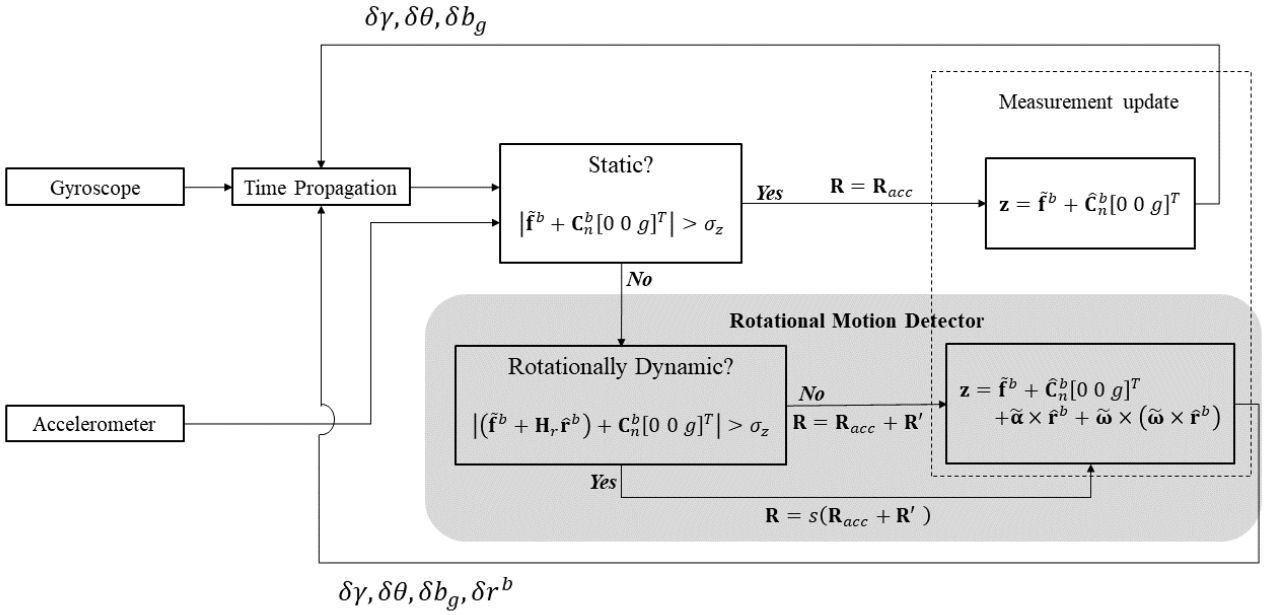

FIGURE 1. Schematic overview of the proposed algorithm.

x, y, z, positions are denoted as r_x, r_y, and r_z, respectively. The estimated center of rotation is augmented to the nominal state vector as follows.

$$\mathbf{x} = \begin{bmatrix} \gamma & \theta | & b_{g,x} & b_{g,y} & b_{g,z} | & r_x & r_y & r_z \end{bmatrix}^T \tag{16}$$

The error state, which we use for our indirect Kalman filter is as follows.

$$\delta\mathbf{x} = \begin{bmatrix} \varphi_N & \varphi_E | & \delta b_{g,x} & \delta b_{g,y} & \delta b_{g,z} | & \delta r_x & \delta r_y & \delta r_z \end{bmatrix}^T \tag{17}$$

The roll, pitch, and gyro bias errors are defined the same as shown in Section II. The augmented center of rotation error is defined as follows.

$$\delta\mathbf{r}^b = \mathbf{r}^b - \hat{\mathbf{r}}^b \tag{18}$$

By including center of rotation into the state vector, the nature of the dynamics can be estimated and explained in terms of any rotational movement that the system might be experiencing. More importantly, the expected effect of such augmentation is improvement in the accuracy of estimating attitude, which we prove experimentally in Section IV.

The Kalman filter equations, including those of time propagation and measurement update, are adopted from [39]. To practice economy, we only present filter properties and equations that deviate from [39].

Expanded from equation (9), the nonlinear continuous augmented state system model is as follows.

System model (nonlinear, continuous):

$$\begin{aligned} \dot{\gamma}, \dot{\theta}, \dot{\boldsymbol{b}}_g \quad & \textit{from equation (9)} \\ \dot{\boldsymbol{r}}^b &= 0 \end{aligned} \tag{19}$$

The augmented error state system model is as follows.

System model (linearized, discrete):

$$\delta\mathbf{x}_k = \boldsymbol{\Phi}_{k-1}\delta\mathbf{x}_{k-1} + \mathbf{w}_{k-1} \tag{20}$$

$$\boldsymbol{\Phi}_k = \mathbf{I}_{8\times8} + \mathbf{F}_k\Delta t, \quad \mathbf{F}_k = \begin{bmatrix} \mathbf{0}_{2\times2} & \mathbf{C}_{1,2r} & \mathbf{0}_{2\times3} \\ \mathbf{0}_{6\times2} & \mathbf{0}_{6\times3} & \mathbf{0}_{6\times3} \end{bmatrix} \tag{21}$$

with process noise covariance matrix, $\mathbf{Q}$, as a diagonal matrix consisted of noise standard deviation of each state. The noise standard deviation for the augmented $\delta\mathbf{r}^b$ is assumed as $10^{-3}\mathrm{m}/\sqrt{\mathrm{Hz}}$. Some literatures suggest that methods such as Runge-Kutta ensure a more accurate discretization than the method we chose in equation (21) [40]. Yet, we use equation (21) instead for three reasons: in the context of a low-grade IMU (such as the IMU used for our experiments in Section IV), the numerical error from the discretization is far smaller than errors from other sources; the discretization error is kept small with a small time-step, Δt [40]; the Runge-Kutta method is computationally heavier than the chosen method.

The *priori* values from performing time propagation of the Kalman filter with above system model, together with the accelerometer measurement, faces the static detector. The static detector determines whether the system is static by comparing the acceleration measurement with the gravity vector with respect to a threshold. If the system is deemed static, the measurement noise covariance matrix is set as $\mathbf{R}_{acc}$, which is $\mathbf{R}$ originating from accelerometer only. Then, measurement update is performed to update only the attitude and the gyroscope bias. The adaptive determination of the measurement noise covariance and the measurement model when deemed static by the static detector are as follows.

Adaptive $\mathbf{R}$:

$$\mathbf{R}_k = \begin{cases} go\ to\ rot.\ detector & if\ \left|\tilde{\mathbf{f}}_k + \hat{\mathbf{C}}_n^b [0 \quad 0 \quad g]^T\right| > \sigma_z \\ \mathbf{R}_{acc} & otherwise \end{cases} \tag{22}$$

Measurement model (linearized, discrete):

$$\delta \mathbf{z}_k = \tilde{\mathbf{f}}_k + \hat{\mathbf{C}}_n^b \begin{bmatrix} 0 & 0 & g \end{bmatrix}^T = \mathbf{H}_k \delta \mathbf{x}_k + \mathbf{v}_k \tag{23}$$

$$\mathbf{H}_k = \begin{bmatrix} \mathbf{C}_{1,2c} & \mathbf{0}_{3\times 6} \end{bmatrix} \tag{24}$$

where σ_z is the measurement noise standard deviation. The above measurement model is similar to the linearized discrete measurement model of equations (13) and (14) from Section II, with the difference being the new observation matrix for our augmented error state vector. As for the threshold of the detectors, we heuristically set it as the measurement noise standard deviation, σ_z, but the value is a user-determined parameter that may be chosen differently. If the threshold is set too low for any of the detectors, it would inflate the measurement covariance matrix; if the threshold is set too high, it would deflate the measurement covariance matrix. Both cases of false detection would hinder the filter from accurately capturing the true dynamics, and thus deteriorate the performance of the proposed algorithm.

However, if deemed dynamic, the system goes through our rotational motion detector. The rotational motion detector checks whether the system is rotationally dynamic by comparing gravity vector with acceleration measurement compensated for the acceleration with respect to the estimated center of rotation. When deemed rotationally static, $\mathbf{R}$ is set as $\mathbf{R}_{acc} + \mathbf{R}'$, where the definition and derivation of $\mathbf{R}'$ is presented in Section III-C. Conversely, when deemed rotationally dynamic, $\mathbf{R}$ is set as $s\left(\mathbf{R}_{acc} + \mathbf{R}'\right)$. The parameter s is a user-set parameter, which we chose as 107 for experiments carried out in this paper. Though very large, the results in Section IV shows that the measurement was still able to influence attitude estimation. The optimal value was chosen through a set of trials. We also confirmed that the degradation of performance due to using other values that are not widely different from the optimal value is minimal. As the system undergoes the rotational motion detector, the measurement update performs an update on not only the attitude and the gyroscope bias, but also the center of rotation. The adaptive determination of the measurement noise covariance and the measurement model of the second step are as follows.

Adaptive $\mathbf{R}$:

$$\mathbf{R}_k = \begin{cases} s\left(\mathbf{R}_{acc} + \mathbf{R}'\right) \\ \quad if\ \left|\left(\tilde{\mathbf{f}}_k + \mathbf{H}_r \hat{\mathbf{r}}^b\right) + \hat{\mathbf{C}}_n^b [0 \quad 0 \quad g]^T\right| > \sigma_z \\ \mathbf{R}_{acc} + \mathbf{R}' \quad otherwise \end{cases} \tag{25}$$

Measurement model (linearized, discrete):

$$\delta \mathbf{z}_k = \tilde{\mathbf{f}}_k + \hat{\mathbf{C}}_n^b \begin{bmatrix} 0 & 0 & g \end{bmatrix}^T + \mathbf{H}_r \hat{\mathbf{r}}^b = \mathbf{H}_k \delta \mathbf{x}_k + \mathbf{v}_k \tag{26}$$

$$\mathbf{H}_k = \begin{bmatrix} \mathbf{C}_{1,2c} & \mathbf{0}_{3\times 3} & \mathbf{H}_r \end{bmatrix} \tag{27}$$

where $\hat{\mathbf{r}}^b$ is the current estimate of the center of rotation in the sensor frame. Also, $\mathbf{H}_r = \left[\tilde{\boldsymbol{\omega}}_k \times\right]^2 + \left[\tilde{\boldsymbol{\alpha}}_k \times\right]$, and $\tilde{\boldsymbol{\alpha}}_k = \frac{\tilde{\boldsymbol{\omega}}_k - \tilde{\boldsymbol{\omega}}_{k-1}}{\Delta t}$, where $\tilde{\boldsymbol{\omega}}_k$ is the tri-axial gyro measurements at time k with following relation.

$$\tilde{\boldsymbol{\omega}}_k = \boldsymbol{\omega}_k + \delta \boldsymbol{\omega}_k \tag{28}$$

From the measurement model shown in equation (26), the centripetal acceleration due to rotational motion about the fixed point at $\mathbf{r}^b$ corresponds to $-\left[\boldsymbol{\omega}_k \times\right]^2 \mathbf{r}^b$, whereas the tangential acceleration corresponds to $-\left[\boldsymbol{\alpha}_k \times\right] \mathbf{r}^b$.

C. DERIVATION OF MEASUREMENT NOISE COVARIANCE MATRIX

With the presence of an error in $\mathbf{H}_r$ from the gyroscope error, the measurement noise covariance matrix $\mathbf{R}_k$ is now larger than conventional measurement noise covariance matrix, $\mathbf{R}_{acc}$. We define the increment as $\mathbf{R}'$, such that

$$\mathbf{R}_k = \mathbf{R}_{acc} + \mathbf{R}' \tag{29}$$

To derive $\mathbf{R}'$, we first define polysemous notations l, m, and n. The notations correspond to numbers 1, 2, or 3 when denoting components of $\mathbf{H}_r$, and correspond to x, y, or z when denoting the axes of gyroscope measurement, $\boldsymbol{\omega}$. To elaborate, in case of $\mathbf{H}_r$ $(2, 3)$, l and m are assigned to y and z axes, and n is automatically assigned to the x axis. Let us define $\delta \mathbf{H}_r\ (l, m)$ to be the error in the (l, m)-th component of $\mathbf{H}_r$. Then, using the definition of $\mathbf{H}_r$, following error expressions can be derived:

$$\delta \mathbf{H}_r\ (l, l) = -\left(\delta \omega_m^2 + \delta \omega_n^2\right) \tag{30}$$

$$\begin{aligned} \delta \mathbf{H}_r\ (l, m \neq l) &= \delta\ (\omega_l \omega_m) + \delta\ (\alpha_n) \\ &= (\tilde{\omega}_l \tilde{\omega}_m + \tilde{\alpha}_n) - (\omega_l \omega_m + \alpha_n) \\ &= \left(\tilde{\omega}_l \tilde{\omega}_m + \frac{\tilde{\omega}_{n,t} - \tilde{\omega}_{n,t-\Delta t}}{\Delta t}\right) \\ &\quad - \left(\omega_l \omega_m + \frac{\omega_{n,t} - \omega_{n,t-\Delta t}}{\Delta t}\right) \\ &= \delta \omega_l \delta \omega_m + \omega_l \delta \omega_m + \omega_m \delta \omega_l \\ &\quad + \frac{\delta \omega_{n,t} - \delta \omega_{n,t-\Delta t}}{\Delta t} \end{aligned} \tag{31}$$

With such derivations of each component of the error matrix, the expectations of squared-error terms are drawn. Their derivations are spanned out for all six cases as followed. In this section we only show the final outcome of each case, and the full process of the derivations are presented in Appendix A.

Case 1:

$$\mathbf{E}\left[\delta \mathbf{H}_r\ (l, l)^2\right] = 8\ (\mathrm{PSD})^2\ \Delta t^2 \tag{32}$$

Case 2:

$$\mathbf{E}\left[\delta \mathbf{H}_r\ (l, m \neq l)^2\right] = (\mathrm{PSD})^2\ \Delta t^2 + \frac{2\ (\mathrm{PSD})^2}{\Delta t^2} + \underbrace{(\omega_l^2 + \omega_m^2)(\mathrm{PSD})\Delta t}_{dependent\ on\ motion} \tag{33}$$

Case 3:

$$\mathbf{E}\left[\delta\mathbf{H}_r\left(l,l\right)\delta\mathbf{H}_r\left(l,m\neq l\right)\right]=0 \tag{34}$$

Case 4:

$$\mathbf{E}\left[\delta\mathbf{H}_r\left(l,l\right)\delta\mathbf{H}_r\left(m\neq l,m\right)\right]=6\left(\mathrm{PSD}\right)^2\Delta t^2 \tag{35}$$

Case 5:

$$\mathbf{E}\left[\delta\mathbf{H}_r\left(l,m\neq l\right)\delta\mathbf{H}_r\left(l,n\neq l\&m\right)\right] = \underbrace{\omega_m\omega_n(\mathrm{PSD})\Delta t+2\omega_l(\mathrm{PSD})}_{\textit{dependent on motion}} \tag{36}$$

Case 6:

$$\mathbf{E}\left[\delta\mathbf{H}_r\left(l,l\right)\delta\mathbf{H}_r\left(m\neq l,n\neq l\&m\right)\right]=0 \tag{37}$$

Assuming that the rotational rate is much smaller than $1/\Delta t$, which corresponds to 100 rad/s for a sampling rate of 100Hz, above six cases can be approximated and reduced down as follows.

For case 2 from above:

$$\mathbf{E}\left[\delta\mathbf{H}_r\left(l,m\neq l\right)^2\right]\approx\frac{2\left(\mathrm{PSD}\right)^2}{\Delta t^2} \tag{38}$$

For all other cases:

$$\mathbf{E}\left[\delta\mathbf{H}_r\left(l,m\right)\delta\mathbf{H}_r\left(n,o\right)\right]\approx 0 \tag{39}$$

Hence, $\mathbf{R}'$, measurement noise covariance matrix induced from the gyroscope error, can be represented as follows.

$$\mathbf{R}'\approx\frac{2\left(\mathrm{PSD}\right)^2}{\Delta t^2}\begin{bmatrix} r_y^2+r_z^2 & r_xr_y & r_zr_x\\ r_xr_y & r_z^2+r_x^2 & r_yr_z\\ r_zr_x & r_yr_z & r_x^2+r_y^2\end{bmatrix} \tag{40}$$

A detailed derivation of $\mathbf{R}'$ is presented in Appendix B. For a gyroscope with amplitude spectral density (ASD) of 0.05 deg/$\sqrt{\mathrm{Hz}}$ sampled at 100Hz, $\sqrt{\frac{2(\mathrm{PSD})^2}{\Delta t^2}}\approx 0.01$ rad/s^2. When $r=\left|\mathbf{r}^b\right|=1$m, this value is comparable to an accelerometer noise with standard deviation of 0.01 m/s^2.

Note that $\mathbf{R}'$ increases as the rotational radius increases. Since the rotational radius during translational motion is conventionally considered infinite, $\mathbf{R}'$ would become infinite under such assumption. This implies that the measurement update of the Kalman filter has practically no effect as $\mathbf{R}_k$ is infinite. Instead, the rotational radius is set to zero, in the sense of resetting the value until the system is under a rotational acceleration again. In the implementation aspect, this is much more practical as $\mathbf{R}_k$ equals to $s\mathbf{R}_{acc}$ under translational motion, meaning the filter still performs an update, just with a larger measurement noise covariance matrix to reflect the dynamicity of the motion. Kinematically speaking, setting the rotational radius to zero does not imply a pure translation, but rather a pure rotation. However, despite the rotational radius being both zero, the proposed algorithm is still able to distinguish between the two motions with its static detector: in a purely translational case, an external acceleration is present, whereas in a purely rotational case, it does not. Furthermore, the outperforming results shown in Section IV also corroborate the validity of our assumption.

D. OBSERVABILITY ANALYSIS

Since proposed algorithm assumes handheld device applications, where dynamics is limited by the maximum speed of human motion, the Piece-Wise Constant System (PWCS) assumption is employed to analyze the observability of the proposed system. The observability matrix for a PWCS [41] is as follows.

$$\mathbf{O}=\begin{bmatrix} O_1\\ O_2\\ \vdots\\ O_r\boldsymbol{\Phi}_{r-1}^{n-1}\boldsymbol{\Phi}_{r-2}^{n-1}\cdots\boldsymbol{\Phi}_1^{n-1}\end{bmatrix}^T \tag{41}$$

where

$$\mathbf{O}_j^T=\begin{bmatrix}\mathbf{H}_j^T & | & \left(\mathbf{H}_j\boldsymbol{\Phi}_j\right)^T & | & \cdots & | & \left(\mathbf{H}_j\boldsymbol{\Phi}_j^{n-1}\right)^T\end{bmatrix} \tag{42}$$

The proposed system is fully observable for rotations about two or more axes. However, for rotations around a single axis, it is only partially observable. In the latter case, the position of center of rotation along the rotation axis is unobservable. We provide detailed derivation and explanation of the observability matrix in Appendix C. Despite the unobservable case, we believe the stability of the system would not be compromised as a circumstance where the rotation axis aligns perfectly with one of the axes is highly unrealistic. We further explain the case with regards to our rate table experiment in Section IV-B.

IV. EXPERIMENTAL RESULTS

To verify the accuracy and robustness of our algorithm, we conduct an extensive evaluation on total of six scenarios, four collected by the authors and two from the benchmark dataset BROAD [36]. In this section, the setups and results of each scenario are presented.

A. SENSOR SETUP AND SCENARIO DESCRIPTIONS

1) AUTHOR-COLLECTED DATASET

The inertial measurement unit (IMU) used to evaluate the proposed attitude estimating algorithm is the Xsens MTx, with its specifications [42] listed in Table 2. As a reference, the VICON infrared camera motion capture system was used to track three markers 10cm apart from one another. However, since VICON only provides attitude values, MTx output was used as acceleration reference. Hence, DCM from VICON attitude multiplied by the gravity vector was deducted from the MTx acceleration value to derive the reference values of the external acceleration. The external acceleration reference is calculated as below:

$$\mathbf{d}_{ref,k}=\tilde{\mathbf{f}}_k-\mathbf{C}_{n_{VICON}}^b\begin{bmatrix}0 & 0 & -g\end{bmatrix}^T \tag{43}$$

A static calibration of gyroscope bias was performed prior to each motion for 20 seconds. The remaining gyro bias after T_{align} seconds of calibration is as follows.

$$\delta b_g=\frac{\sigma_{gyr}}{\sqrt{T_{align}}}\approx 0.01\mathrm{deg/s} \tag{44}$$

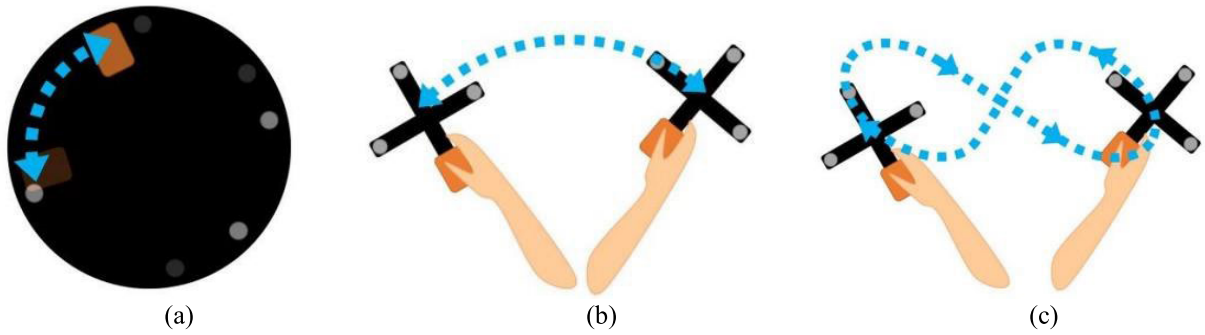

FIGURE 2. Schematic view of (a) the rate table, (b) "Handheld Yaw", and (c) "Handheld Eight" scenarios. The orange objects are the IMUs in use.

where σ_{gyr} is the noise standard deviation of the gyroscope. Above value was used in setting the initial gyroscope bias error covariance.

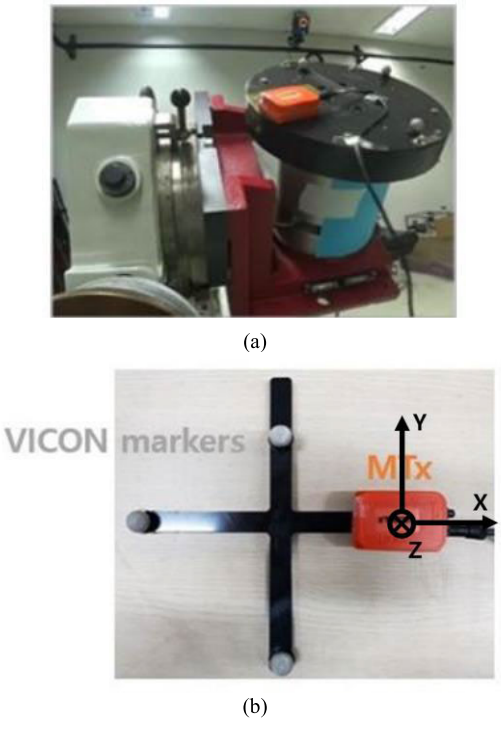

FIGURE 3. Setup of (a) the rate table and (b) the handheld experiments.

TABLE 2. MTx specifications.

	Gyroscope	Accelerometer
Measurement range	± 1200 deg/s	± 5g
Sampling rate	100Hz	
Noise density	0.05 deg/s/$\sqrt{\text{Hz}}$	200 μg/$\sqrt{\text{Hz}}$

Of the four tested scenarios, the first two were rate table experiments with different rates. The setup of the rate table experiments is as shown in Fig. 3 (a). We call the first scenario as "Rate Table Slow" and the second scenario as "Rate Table Fast." Both scenarios involved periodic bang-bang maneuvers, depicted in Fig. 2 (a), with trapezoidal velocity profiles. For "Rate Table Slow," the average and maximum norm deviations from static acceleration was 0.54m/s^2 and 1.03 m/s^2, respectively. For "Rate Table Fast," the average and maximum norm deviations from static acceleration was 1.25 m/s^2 and 1.95 m/s^2, respectively.

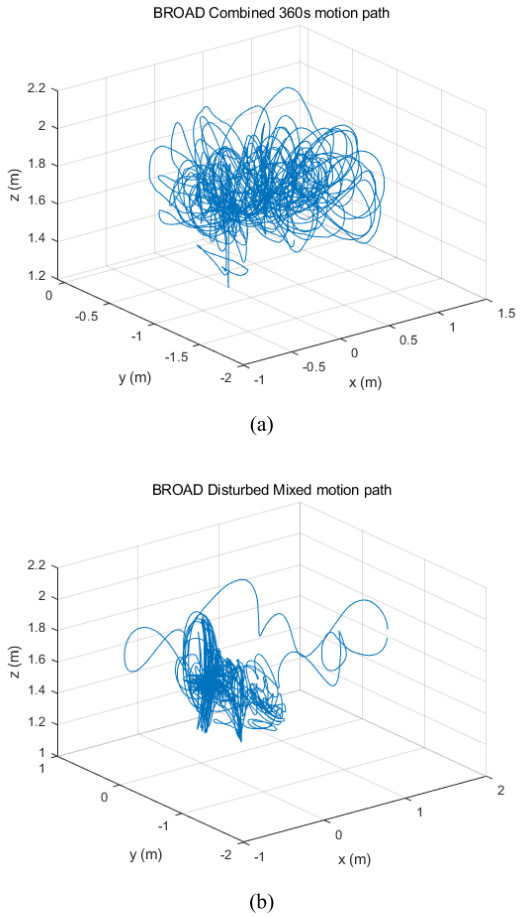

FIGURE 4. 3D motion paths of (a) the "BROAD Combined 360s" and (b) the "BROAD Disturbed Mixed" experiments.

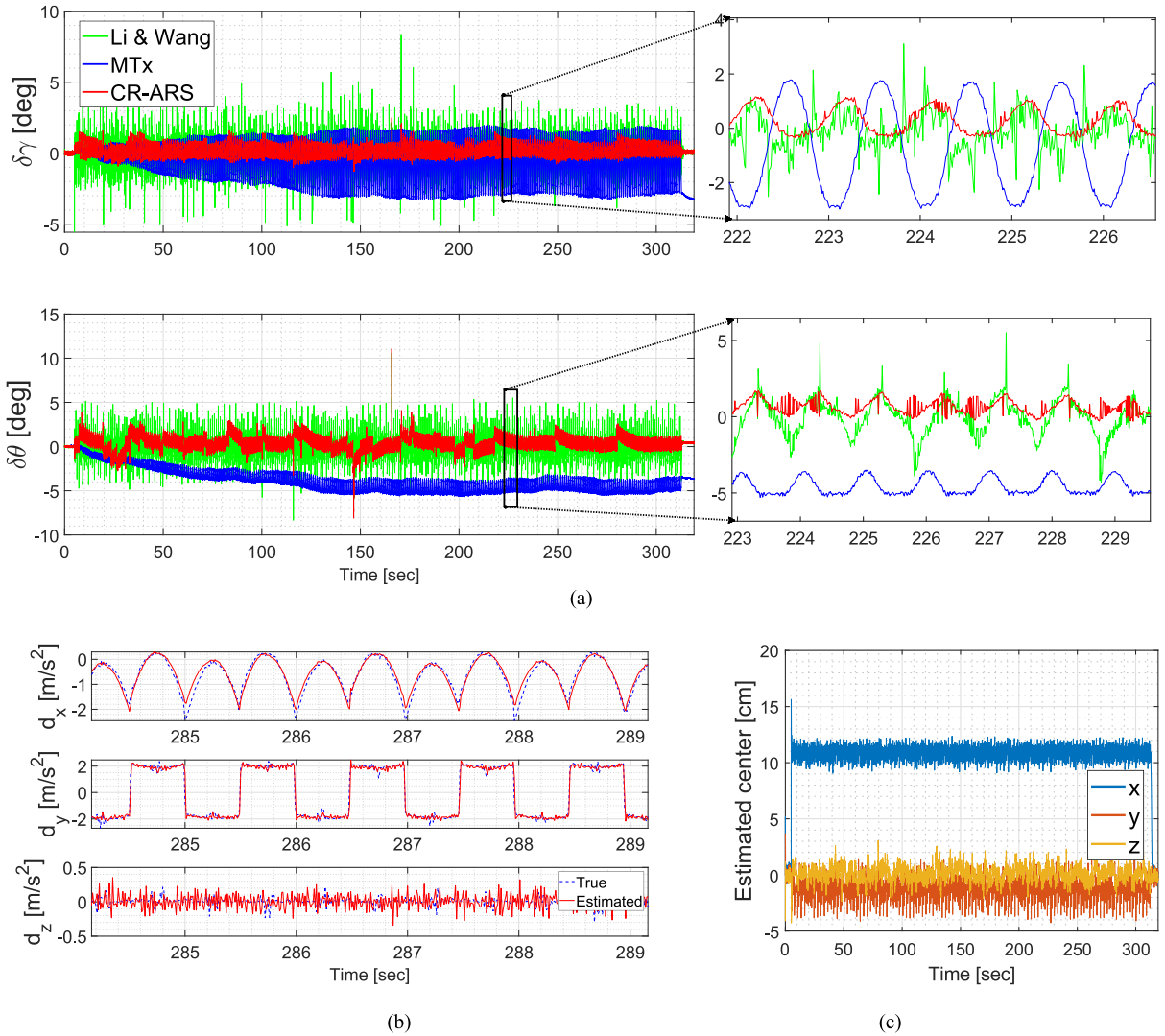

FIGURE 5. Results of a single trial of "Rate Table Fast". (a) Errors of estimated attitude, (b) estimated external acceleration, and (c) estimated center of rotation. From (a), the conventional method, MTx output, and the proposed method are colored in green, blue, and red, respectively, denoted as "Li & Wang", "MTx", and "CR-ARS" (short for Center-of-Rotation based ARS), respectively.

TABLE 3. Myon Aktos-t specifications.

	Gyroscope	Accelerometer
Measurement range	± 2000 deg/s	± 16g
Sampling rate	286Hz	
Noise standard deviation	0.10 deg/s	0.056 m/s^2

The latter two were handheld experiments to demonstrate performance in actual usage. The setup of the handheld experiments is as shown in Fig. 3 (b). The third scenario involved high-dynamic forearm rotations about the vertical axis, as in Fig. 2 (b). We call this scenario "Handheld Yaw." The average norm deviation from static acceleration was 7.46 m/s^2, and at times it reached up to 31.18 m/s^2. The fourth and last scenario involved high-dynamic swings in figure-of-eight curves, as in Fig. 2 (c). The motion is similar to putting an elbow on a table and drawing and "X" with the fist, resulting in a trajectory comprised of two arcs with the center as the elbow. We call this scenario "Handheld Eight." The average acceleration norm deviation from the gravity was 3.87 m/s^2, and at times it reached up to 12.39 m/s^2. All four sequences have fixed center of rotation and are comprised of primarily rotational motion to highlight the efficacy of our contribution. We present quantitative results for all sequences, but only provide full graphical representation for "Rate Table Fast" and "Handheld Eight" to practice economy.

2) BROAD DATASET [36]

BROAD dataset [36] is comprised of 39 trials that vary in types of motions, the speeds of motions, and existence

of accelerometer and/or magnetometer disturbances. All trials were recorded with 9-axis IMU Myon Aktos-t from Myon AG, Switzerland, with its specifications [36] listed in Table 3. For the ground truth data, an Optitrack OMC system of eight cameras was used, providing angular accuracy of 0.2 degrees [36].

Of the 39 trials, we chose two, the 20th and the 39th, to evaluate our algorithm on real-world scenarios of complex motions and with varying center of rotation. The former is an undisturbed trial with combination of rotational and translational motions lasting 360 seconds, named "BROAD Combined 360s" hereafter. The sequence goes under average acceleration norm of 4.00 m/s^2 and maximum of 11.70 m/s^2. The latter, named "BROAD Disturbed Mixed" hereafter, is a trial of 280 seconds with disturbed and undisturbed phases coexisting. The trial is comprised of several segments of combined motion of rotation and translation with short breaks in between. The sequence goes under average acceleration norm of 3.25 m/s^2 and maximum of 40.22 m/s^2. Unlike our author-collected datasets, the chosen BROAD trials present more complex motions closer to real-world situations with varying center of rotation, shown by their 3D motion paths in Fig. 4, thus appropriate for evaluating robustness of our proposed algorithm.

For all experiments, the performance evaluation was conducted in terms of root mean square error (RMSE). For fair comparison, an algorithm, referred to as "conventional" hereafter, was devised, adopting measurement noise covariance adaptation scheme based on the work of Li and Wang [14], combined with the states and filter structure described in Section II. Hence, for attitude estimation, the proposed algorithm was compared with the conventional algorithm and the MTx output, whereas for external acceleration estimation, it was only compared with the conventional algorithm as the MTx output was used to derive the reference value, as explained earlier in this section. Since the BROAD dataset does not provide attitude output by Myon Aktos-t, we compare only with the conventional algorithm for the two BROAD trials.

TABLE 4. RMSE results of Rate Table Slow.

Trial No.	Roll [deg]			Pitch [deg]			Ext. Acc. [m/s^2]	
	Conv.	MTx	Prop.	Conv.	MTx	Prop.	Conv.	Prop.
1	0.54	1.48	**0.37**	**0.59**	2.83	0.68	0.98	**0.19**
2	0.55	1.64	**0.42**	0.64	3.61	**0.60**	0.97	**0.19**
3	0.57	1.86	**0.39**	0.64	3.91	**0.53**	0.97	**0.19**
4	0.55	1.69	**0.40**	0.63	3.48	**0.57**	0.97	**0.18**

B. RATE TABLE EXPERIMENTS

The results of "Rate Table Slow" scenario are summarized in Table 4. The proposed algorithm outperforms both the conventional algorithm and MTx in most cases of attitude estimation, the former by 20-30%, though the conventional algorithm also shows satisfactory results of sub-degree error. For external acceleration estimation, the proposed outperforms the conventional algorithm in all trials by far, showing 80% less error.

TABLE 5. RMSE results of Rate Table Fast.

Trial No.	Roll [deg]			Pitch [deg]			Ext. Acc. [m/s^2]	
	Conv.	MTx	Prop.	Conv.	MTx	Prop.	Conv.	Prop.
1	1.08	1.57	**0.91**	3.53	3.89	**3.01**	2.15	**0.27**
2	0.48	1.08	**0.38**	**0.86**	4.08	0.87	2.11	**0.23**
3	1.13	2.35	**0.77**	2.02	3.76	**1.72**	2.24	**0.21**
4	0.98	1.86	**0.65**	1.79	4.15	**1.49**	2.08	**0.30**

TABLE 6. RMSE results of Handheld Yaw.

Trial No.	Roll [deg]			Pitch [deg]			Ext. Acc. [m/s^2]	
	Conv.	MTx	Prop.	Conv.	MTx	Prop.	Conv.	Prop.
1	1.73	0.82	**0.75**	0.47	0.56	**0.40**	11.90	**4.23**
2	1.94	1.17	**1.00**	0.48	**0.31**	0.48	12.58	**4.27**
3	2.17	**0.67**	0.69	0.49	0.71	**0.40**	18.15	**5.61**
4	1.45	0.54	**0.47**	0.49	0.57	**0.34**	12.99	**3.81**

TABLE 7. RMSE results of Handheld Eight.

Trial No.	Roll [deg]			Pitch [deg]			Ext. Acc. [m/s^2]	
	Conv.	MTx	Prop.	Conv.	MTx	Prop.	Conv.	Prop.
1	1.26	4.58	**0.76**	**0.59**	1.68	0.69	5.75	**2.52**
2	1.88	2.14	**0.99**	0.54	2.19	**0.50**	7.32	**2.71**
3	1.57	2.36	**0.78**	0.73	1.91	**0.62**	7.02	**2.74**
4	1.96	3.51	**0.81**	0.86	2.84	**0.75**	8.01	**2.62**

Table 5 summarizes the results of "Rate Table Fast" scenario. Similar to the previous scenario, the proposed algorithm outperforms both the conventional algorithm and MTx in most cases of attitude estimation. For external acceleration estimation, the proposed outperforms the conventional algorithm in all trials by an even greater discrepancy than the previous scenario. Fig. 5 (a) shows a full graphical comparison of attitude estimation of a single trial. Estimated external acceleration of a single trial compared to the reference value, magnified to show results of 5 seconds, is shown in Fig. 5 (b). Similar to previous scenario, it can be seen that our proposed algorithm presents superb performance of 88% less error on average. The estimated center of rotation is shown in Fig. 5 (c). The sensor was indeed attached 10cm from the center of the rate table, indicating that the algorithm

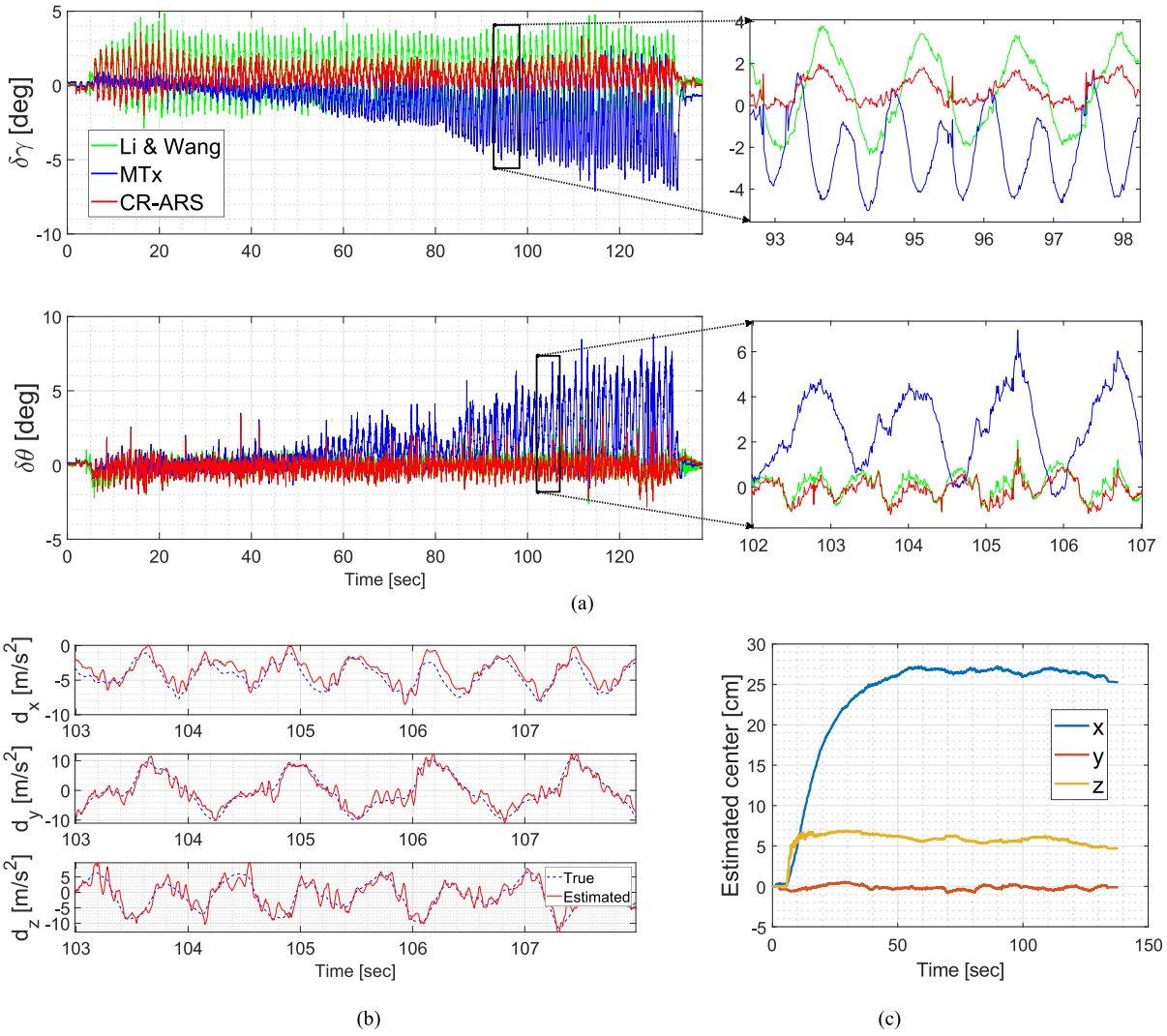

FIGURE 6. Results of a single trial of "Handheld Eight". (a) Errors of estimated attitude, (b) estimated external acceleration, and (c) estimated center of rotation. From (a), the conventional method, MTx output, and the proposed method are colored in green, blue, and red, respectively, denoted as "Li & Wang", "MTx", and "CR-ARS" (short for Center-of-Rotation based ARS), respectively.

has successfully estimated the center of rotation. Though accurate estimation of center of rotation itself is not the focus of this research, such accuracy undoubtedly improves the performance of the filter.

TABLE 8. RMSE Results of BROAD dataset.

Dataset	Roll [deg]		Pitch [deg]		Ext. Acc. [m/s^2]	
	Conv.	Prop.	Conv.	Prop.	Conv.	Prop.
Combined 360s	0.91	**0.58**	0.59	**0.36**	0.82	**0.36**
Disturbed Mixed	1.24	**0.88**	0.98	**0.65**	2.49	**1.06**

Our rate table experiments might be considered as rotations around a single axis, which is the unobservable case mentioned in Section III-D. Yet, as seen in Fig. 5 (c), the rotation axis and the z-axis are not perfectly aligned, and the results prove that the stability of the system is not compromised by the partially observable nature of the system.

C. HANDHELD EXPERIMENTS

The results of "Handheld Yaw" scenario are summarized in Table 6. For roll estimation, our proposed algorithm demonstrates the best results of near sub-degree error, while MTx shows comparable performance. The proposed algorithm also shows best performance on pitch estimation, while all three methods show performance of sub-degree error. In case of external acceleration estimation, the proposed greatly outperforms the conventional method with 68% less error. Considering that "Handheld Yaw" is the most dynamic of all four scenarios, it is proven that our algorithm indeed delivers superb performance, withstanding such harsh and challenging conditions. Compared to the rate table experiments, the

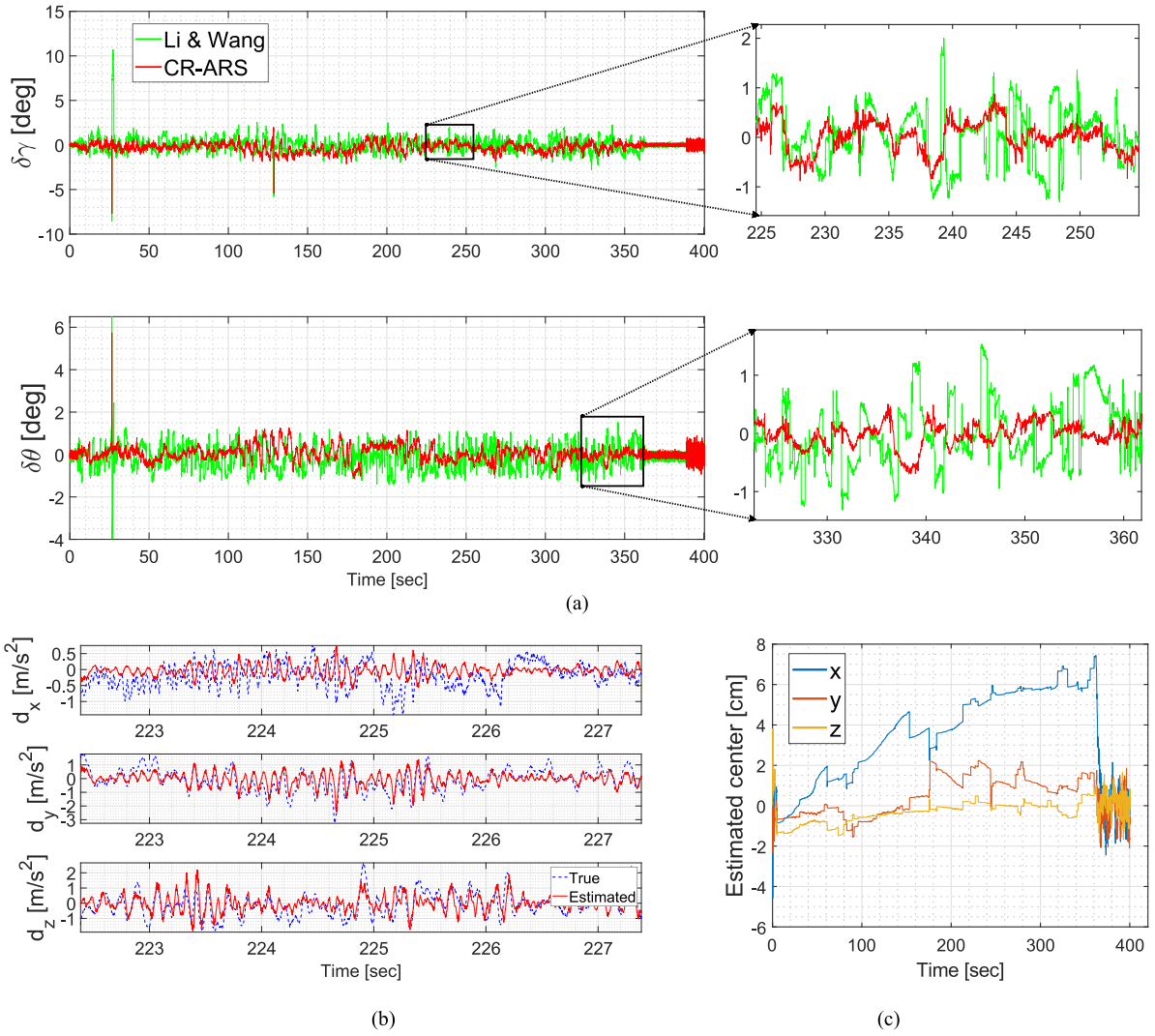

FIGURE 7. Results of a single trial of "BROAD Combined 360s". (a) Errors of estimated attitude, (b) estimated external acceleration, and (c) estimated center of rotation. From (a), the conventional method and the proposed method are colored in green and red, respectively, denoted as "Li & Wang" and "CR-ARS" (short for Center-of-Rotation based ARS), respectively.

accuracy of estimating external acceleration is compromised due to harsh nature of the motion. Yet, our algorithm still outperforms the conventional algorithm by a great deal, proving improved robustness towards harsh motion.

The results of "Handheld Eight" scenario are summarized in Table 7. Our proposed method outperforms both conventional and MTx results in most cases, with sub-degree error for both roll and pitch of all four trials. As for estimating external acceleration, proposed algorithm shows better performance compared to the conventional algorithm with 62% less error, consistent with the results of other scenarios. Together with the results from "Handheld Yaw", we can confidently claim that our method successfully estimates attitude and external acceleration in highly dynamic conditions, especially with motions regarding center of rotation. A graphical comparison of attitude estimation of a single trial is presented in Fig. 6 (a). Fig. 6 (c) shows estimated center of rotation of this scenario. When compared to other scenarios, it can be noted that the estimation has a delay in converging to accurate value of center of rotation, which is the length of the forearm. Such delay can explain a slightly higher error within the timeframe of 0-40 seconds than the rest of the time, shown in Fig. 6 (a). Finally, Fig. 6 (b) shows estimated external acceleration of a single trial compared to the reference value, magnified for 5 seconds.

D. BROAD DATASET

The results of "BROAD Combined 360s" scenario are summarized in the first row of Table 8. Our proposed method outperforms the conventional algorithm by 38%, with sub-degree error for both roll and pitch. A graphical comparison of attitude estimation of a single trial is presented in Fig. 7 (a). The accuracy of estimating external acceleration is also improved compared to the conventional method,

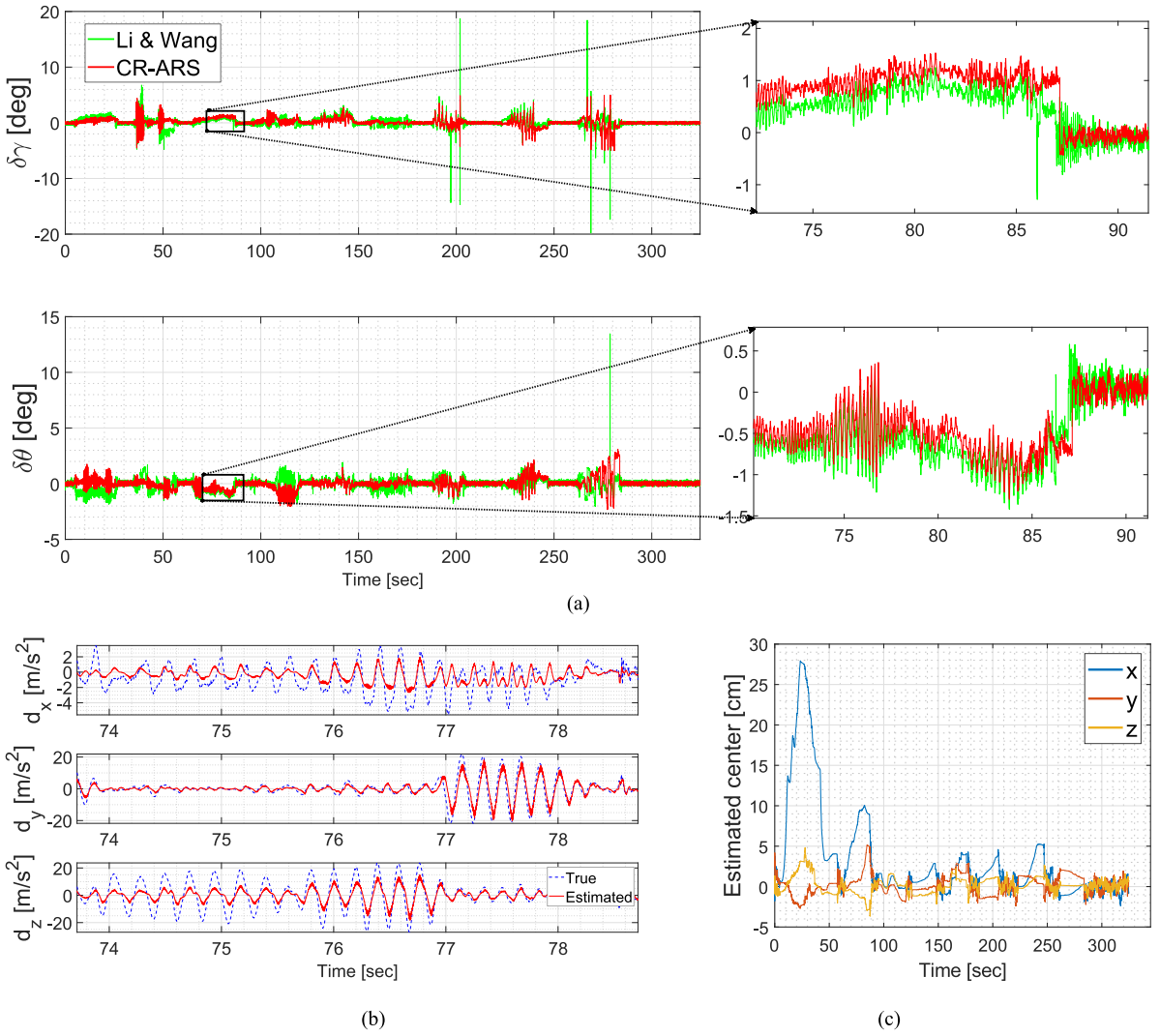

FIGURE 8. Results of a single trial of "BROAD Disturbed Mixed". (a) Errors of estimated attitude, (b) estimated external acceleration, and (c) estimated center of rotation. From (a), the conventional method and the proposed method are colored in green and red, respectively, denoted as "Li & Wang" and "CR-ARS" (short for Center-of-Rotation based ARS), respectively.

showing 56% less error, consistent with the results of author-collected scenarios. Fig. 7 (c) shows estimated center of rotation of this scenario. When compared to the previous author-collected dataset, it can be seen that the center of rotation changes irregularly, hence proving that estimating center of rotation online serves a purpose in situations with arbitrary motions. Fig. 7 (b) shows estimated external acceleration compared to the reference value, magnified for 5 seconds.

The second row of Table 8 presents the results of ''BROAD Disturbed Mixed'' scenario. The results show that our method outperforms the conventional method by 32% in attitude estimation. A full graphical representation of attitude estimation is presented in Fig. 8 (a). Our algorithm also outperforms the conventional in estimating external acceleration with 57% less error. Fig. 8 (b) shows estimated external acceleration of a single trial compared to the reference value, magnified for 5 seconds. From the graph, we can see that there has been a false detection of external acceleration from 74 to 77 second of the sequence. Judging from the provided sensor data, this deviation can be explained by a sudden change in the gyroscope measurements within that window, which results in an erroneous deduction of the gravity vector. Such false detection leads to deterioration of accuracy in attitude estimation, as explained in Section III-B. The zoomed graph of Fig. 8 (a) corroborates the effect of false detection, showing increased attitude estimation error for both roll and pitch. However, it is also shown that false detection does not have a lasting effect on degradation of performance as the error normalizes when the filter starts to correctly detect external acceleration. Lastly, the estimated center of rotation is shown in Fig. 8 (c). We prove once again that our method estimates center of rotation well through the areas with near-zero values, which coincide with the intermittent short breaks between the dynamic phases that ''BROAD Disturbed Mixed'' has.

The evaluation on both BROAD sequences effectively demonstrate the robustness of our algorithm, proving that the applicability of our method is not limited to situations with rotation-only motions or a fixed center of rotation.

V. CONCLUSION

In this work, we presented an augmented Kalman filter-based ARS that accurately estimates attitude with center of rotation augmented to its error-state vector.

As an accurate estimation of the external acceleration is a key to a successful ARS, knowing the types of undergoing motion is crucial. The augmentation of center of rotation precisely does that: estimated center of rotation allows us to describe the motion with respect to rotational motions as well as translational ones, unlike previous works that do not distinguish whether the motion is translational, rotational, or both.

With a more specific understanding of the motion, we employ two motion detectors to adaptively adopt a measurement model and noise covariance matrix more fitting to the undergoing motion. The static detector, the first of the two detectors, is similar to those of the conventional threshold-based algorithms: determining whether the system is static or not, without considering the nature of the dynamicity. The superiority of our algorithm lies with the second detector, the rotational motion detector. Effectively taking advantage of the estimated center of rotation, the detector not only distinguishes whether the dynamicity of the system inherits a rotational motion but also provides the filter with a more accurate measurement model that incorporates rotational acceleration. This includes a newly defined component of the measurement noise covariance matrix, $\mathbf{R}'$, with its full derivation thoroughly presented in Section III-C, Appendix A and Appendix B.

Our algorithm is validated through author-collected experiments and existing benchmark dataset [36] in Section IV. The former is comprised of four experiments: ''Rate Table Slow'', ''Rate Table Fast'', ''Handheld Yaw'', and ''Handheld Eight''. These experiments are intended to highlight the contribution as they are almost purely rotational with fixed center of rotation. With the estimated center of rotation and the rotational motion detector, the proposed algorithm outperforms the conventional algorithm and the MTx output in terms of accuracy in estimating the attitude and the external acceleration in almost all sequences. From the benchmark dataset, we chose two sequences, ''BROAD Combined 360s'' and ''BROAD Disturbed Mixed'', to prove the robustness of our algorithm against challenging situations. The sequences consist complex motions, in combination of translational and rotational motions with varying center of rotation. Even in such adverse circumstances, our algorithm outperformed the conventional method with sub-degree errors, proving that the superb performance of the proposed algorithm is not limited to purely rotational motion with fixed center of rotation.

This work may be extended to an ARS for robot applications or generally for any dynamic system, preferably with unknown model parameters and/or under rotational motions. For future work, the relationship between the magnitude of acceleration and performance can be further investigated through additional experiments.

APPENDIX A
DERIVATION OF EXPECTATIONS OF SQUARED-ERROR TERMS

Case 1:

$$\begin{aligned}
&\mathbf{E}\left[\delta\mathbf{H}_r\,(l,l)^2\right] \\
&\quad= \mathbf{E}\left[\,\delta\omega_m^4+\delta\omega_n^4+2\delta\omega_m^2\delta\omega_n^2\,\right] \\
&\quad= \mathbf{E}\left[\delta\omega_m^4\right]+\mathbf{E}\left[\delta\omega_n^4\right]+2\mathbf{E}\left[\delta\omega_m^2\right]\mathbf{E}\left[\delta\omega_n^2\right] \\
&\qquad\qquad (\because\ \delta\omega_m \& \delta\omega_n\ \textit{indep.}) \\
&\quad= 3\sigma^4+3\sigma^4+2\sigma^4 \\
&\quad= 8\sigma^4 \\
&\quad= 8\,(\mathrm{PSD})^2\,\Delta t^2
\end{aligned}$$

Case 2:

$$\begin{aligned}
&\mathbf{E}\left[\delta\mathbf{H}_r\,(l,m\neq l)^2\right] \\
&= \mathbf{E}\left[\begin{array}{c}\delta\omega_l^2\delta\omega_m^2+\omega_l^2\delta\omega_m^2+\omega_m^2\delta\omega_l^2+\dfrac{\delta\omega_{n,t}^2+\delta\omega_{n,t-\Delta t}^2}{\Delta t^2} \\ +(\textit{terms containing } \delta\omega \textit{ to odd powers})\end{array}\right] \\
&= \mathbf{E}\left[\delta\omega_l^2\right]\mathbf{E}\left[\delta\omega_m^2\right]+\omega_l^2\mathbf{E}\left[\delta\omega_m^2\right]+\omega_m^2\mathbf{E}\left[\delta\omega_l^2\right] \\
&\quad+\frac{\mathbf{E}\left[\delta\omega_{n,t}^2\right]+\mathbf{E}\left[\delta\omega_{n,t-\Delta t}^2\right]}{\Delta t^2} \\
&= \sigma^4+\omega_l^2\sigma^2+\omega_m^2\sigma^2+\frac{\sigma^2+\sigma^2}{\Delta t^2} \\
&= \sigma^4+\left(\omega_l^2+\omega_m^2+\frac{2}{\Delta t^2}\right)\sigma^2 \\
&= (\mathrm{PSD})^2\,\Delta t^2+\frac{2\,(\mathrm{PSD})^2}{\Delta t^2}+\underbrace{(\omega_l^2+\omega_m^2)(\mathrm{PSD})\Delta t}_{\textit{dependent on motion}}
\end{aligned}$$

Case 3:

$$\begin{aligned}
&\mathbf{E}\left[\delta\mathbf{H}_r\,(l,l)\,\delta\mathbf{H}_r\,(l,m\neq l)\right] \\
&\quad= \mathbf{E}\left[\,\textit{all terms containing } \delta\omega \textit{ to odd powers}\,\right] \\
&\quad= 0
\end{aligned}$$

Case 4:

$$\begin{aligned}
&\mathbf{E}\left[\delta\mathbf{H}_r\,(l,l)\,\delta\mathbf{H}_r\,(m\neq l,m)\right] \\
&\quad= \mathbf{E}\left[\begin{array}{c}\delta\omega_m^2\delta\omega_l^2+\delta\omega_m^2\delta\omega_n^2+\delta\omega_l^2\delta\omega_n^2+\delta\omega_n^4 \\ +(\textit{terms containing } \delta\omega \textit{ to odd powers})\end{array}\right] \\
&\quad= \mathbf{E}\left[\delta\omega_m^2\right]\mathbf{E}\left[\delta\omega_l^2\right]+\mathbf{E}\left[\delta\omega_m^2\right]\mathbf{E}\left[\delta\omega_n^2\right] \\
&\qquad+\mathbf{E}\left[\delta\omega_l^2\right]\mathbf{E}\left[\delta\omega_n^2\right]+\mathbf{E}\left[\delta\omega_n^4\right] \\
&\quad= \sigma^4+\sigma^4+\sigma^4+3\sigma^4 \\
&\quad= 6\sigma^4 \\
&\quad= 6\,(\mathrm{PSD})^2\,\Delta t^2
\end{aligned}$$

Case 5:

$$\begin{aligned}
&\mathbf{E}\left[\delta\mathbf{H}_r\left(l, m\neq l\right)\delta\mathbf{H}_r\left(l, n\neq l\&m\right)\right]\\
&= \mathbf{E}\left[\begin{array}{l}\omega_m\omega_n\delta\omega_l^2 + \dfrac{\omega_l\delta\omega_m^2}{\Delta t} + \dfrac{\omega_l\delta\omega_n^2}{\Delta t}\\ +\left(\textit{terms containing } \delta\omega \textit{ to odd powers}\right)\end{array}\right]\\
&= \omega_m\omega_n\mathbf{E}\left[\delta\omega_l^2\right] + \frac{\omega_l}{\Delta t}\mathbf{E}\left[\delta\omega_m^2\right] + \frac{\omega_l}{\Delta t}\mathbf{E}\left[\delta\omega_n^2\right]\\
&= \omega_m\omega_n\sigma^2 + \frac{2\omega_l\sigma^2}{\Delta t}\\
&= \underbrace{\omega_m\omega_n(\mathrm{PSD})\Delta t + 2\omega_l(\mathrm{PSD})}_{\textit{dependent on motion}}
\end{aligned}$$

Case 6:

$$\begin{aligned}
&\mathbf{E}\left[\delta\mathbf{H}_r\left(l, l\right)\delta\mathbf{H}_r\left(m\neq l, n\neq l\&m\right)\right]\\
&\quad= \mathbf{E}\left[\textit{all terms containing } \delta\omega \textit{ to odd powers}\right]\\
&\quad= 0
\end{aligned}$$

APPENDIX B
DERIVATION OF R'

$\mathbf{R}'$ is the measurement noise covariance matrix induced from the gyroscope error, or more specifically, from the $\mathbf{H}_r\hat{\mathbf{r}}^b$ of the measurement equation (26). In Kalman filter, the measurement noise covariance matrix is the expectation of the error squared. Accordingly, R′ can be expressed as $\mathrm{E}\left[\left(\delta\mathbf{H}_r\hat{\mathbf{r}}^b\right)\left(\delta\mathbf{H}_r\hat{\mathbf{r}}^b\right)^T\right]$. Expansion of this is shown as follows.

$$\begin{aligned}
&\mathrm{E}\left[\left(\delta\mathbf{H}_r\hat{\mathbf{r}}^b\right)\left(\delta\mathbf{H}_r\hat{\mathbf{r}}^b\right)^T\right]\\
&= \mathrm{E}\left[\begin{bmatrix}\delta\mathbf{H}_r(1,1)\cdot r_x + \delta\mathbf{H}_r(1,2)\cdot r_y + \delta\mathbf{H}_r(1,3)\cdot r_z\\ \delta\mathbf{H}_r(2,1)\cdot r_x + \delta\mathbf{H}_r(2,2)\cdot r_y + \delta\mathbf{H}_r(2,3)\cdot r_z\\ \delta\mathbf{H}_r(3,1)\cdot r_x + \delta\mathbf{H}_r(3,2)\cdot r_y + \delta\mathbf{H}_r(3,3)\cdot r_z\end{bmatrix}\right.\\
&\quad\left.\cdot\begin{bmatrix}\delta\mathbf{H}_r(1,1)\cdot r_x + \delta\mathbf{H}_r(1,2)\cdot r_y + \delta\mathbf{H}_r(1,3)\cdot r_z\\ \delta\mathbf{H}_r(2,1)\cdot r_x + \delta\mathbf{H}_r(2,2)\cdot r_y + \delta\mathbf{H}_r(2,3)\cdot r_z\\ \delta\mathbf{H}_r(3,1)\cdot r_x + \delta\mathbf{H}_r(3,2)\cdot r_y + \delta\mathbf{H}_r(3,3)\cdot r_z\end{bmatrix}^T\right]
\end{aligned}$$

From equations (38) and (39), the above equation is only left with the $\delta\mathbf{H}_r\left(l, m\neq l\right)^2$ terms, as shown below.

$$\mathrm{E}\left[\left(\delta\mathbf{H}_r\hat{\mathbf{r}}^b\right)\left(\delta\mathbf{H}_r\hat{\mathbf{r}}^b\right)^T\right] = \begin{bmatrix}\boldsymbol{v}_1 & \boldsymbol{v}_2 & \boldsymbol{v}_3\end{bmatrix}$$

where

$$\boldsymbol{v}_1 = \begin{bmatrix}\delta\mathbf{H}_r\left(l, m\neq l\right)^2\cdot r_y^2 + \delta\mathbf{H}_r\left(l, m\neq l\right)^2\cdot r_z^2\\ \delta\mathbf{H}_r\left(l, m\neq l\right)^2\cdot r_x r_y\\ \delta\mathbf{H}_r\left(l, m\neq l\right)^2\cdot r_z r_x\end{bmatrix}$$

$$\boldsymbol{v}_2 = \begin{bmatrix}\delta\mathbf{H}_r\left(l, m\neq l\right)^2\cdot r_x r_y\\ \delta\mathbf{H}_r\left(l, m\neq l\right)^2\cdot r_z^2 + \delta\mathbf{H}_r\left(l, m\neq l\right)^2\cdot r_x^2\\ \delta\mathbf{H}_r\left(l, m\neq l\right)^2\cdot r_y r_z\end{bmatrix}$$

$$\boldsymbol{v}_3 = \begin{bmatrix}\delta\mathbf{H}_r\left(l, m\neq l\right)^2\cdot r_z r_x\\ \delta\mathbf{H}_r\left(l, m\neq l\right)^2\cdot r_y r_z\\ \delta\mathbf{H}_r\left(l, m\neq l\right)^2\cdot r_x^2 + \delta\mathbf{H}_r\left(l, m\neq l\right)^2\cdot r_y^2\end{bmatrix}$$

Hence, we can conclude by simplifying the above:

$$\begin{aligned}
\mathbf{R}' &= \mathrm{E}\left[\left(\delta\mathbf{H}_r\hat{\mathbf{r}}^b\right)\left(\delta\mathbf{H}_r\hat{\mathbf{r}}^b\right)^T\right]\\
&= \mathrm{E}\left[\delta\mathbf{H}_r\left(l, m\neq l\right)^2\right]\begin{bmatrix}r_y^2+r_z^2 & r_x r_y & r_z r_x\\ r_x r_y & r_z^2+r_x^2 & r_y r_z\\ r_z r_x & r_y r_z & r_x^2+r_y^2\end{bmatrix}\\
&= \frac{2\left(\mathrm{PSD}\right)^2}{\Delta t^2}\begin{bmatrix}r_y^2+r_z^2 & r_x r_y & r_z r_x\\ r_x r_y & r_z^2+r_x^2 & r_y r_z\\ r_z r_x & r_y r_z & r_x^2+r_y^2\end{bmatrix}
\end{aligned}$$

APPENDIX C
DETAILS ON THE OBSERVABILITY MATRIX

We first conduct full expansions of $\mathbf{H}$ and $\boldsymbol{\Phi}$.

$$\mathbf{H} = \begin{bmatrix}\mathbf{C}_{1,2c} & \mathbf{0}_{3\times3} & \mathbf{H}_r\end{bmatrix}$$

$$\begin{aligned}
\mathbf{C}_{1,2c} &= \textit{first two columns of } \mathbf{C}_n^b\left[\mathbf{g}\times\right]\\
&= \mathbf{C}_n^b\begin{bmatrix}0 & -g\\ g & 0\\ 0 & 0\end{bmatrix}\\
&= \begin{bmatrix}\mathbf{C}_n^b(1,2)\,g & -\mathbf{C}_n^b(1,1)\,g\\ \mathbf{C}_n^b(2,2)\,g & -\mathbf{C}_n^b(2,1)\,g\\ \mathbf{C}_n^b(3,2)\,g & -\mathbf{C}_n^b(3,1)\,g\end{bmatrix}
\end{aligned}$$

$$\begin{aligned}
\mathbf{H}_r &= \left[\tilde{\boldsymbol{\omega}}\times\right]^2 + \left[\tilde{\boldsymbol{\alpha}}\times\right]\\
&= \begin{bmatrix}-\left(\omega_y^2+\omega_z^2\right) & \omega_x\omega_y & \omega_x\omega_x\\ \omega_x\omega_y & -\left(\omega_z^2+\omega_x^2\right) & \omega_y\omega_z\\ \omega_z\omega_x & \omega_y\omega_z & -\left(\omega_x^2+\omega_y^2\right)\end{bmatrix}\\
&\quad+\begin{bmatrix}0 & -\boldsymbol{\alpha}_z & \boldsymbol{\alpha}_y\\ \boldsymbol{\alpha}_z & 0 & -\boldsymbol{\alpha}_x\\ -\boldsymbol{\alpha}_y & \boldsymbol{\alpha}_x & 0\end{bmatrix}\\
&= \begin{bmatrix}\boldsymbol{v}_4 & \boldsymbol{v}_5 & \boldsymbol{v}_6\end{bmatrix}
\end{aligned}$$

where

$$\boldsymbol{v}_4 = \begin{bmatrix}\omega_x\omega_y\boldsymbol{\alpha}_z - \omega_z\omega_x\boldsymbol{\alpha}_y\\ -\left(\omega_z^2+\omega_x^2\right)\boldsymbol{\alpha}_z - \omega_y\omega_z\boldsymbol{\alpha}_y\\ \omega_y\omega_z\boldsymbol{\alpha}_z + \left(\omega_z^2+\omega_x^2\right)\boldsymbol{\alpha}_y\end{bmatrix}$$

$$\boldsymbol{v}_5 = \begin{bmatrix}\left(\omega_y^2+\omega_z^2\right)\boldsymbol{\alpha}_z + \omega_x\omega_y\boldsymbol{\alpha}_x\\ -\omega_x\omega_y\boldsymbol{\alpha}_z + \omega_y\omega_z\boldsymbol{\alpha}_x\\ -\omega_z\omega_x\boldsymbol{\alpha}_z - \left(\omega_x^2+\omega_y^2\right)\boldsymbol{\alpha}_x\end{bmatrix}$$

$$\boldsymbol{v}_6 = \begin{bmatrix}-\left(\omega_y^2+\omega_z^2\right)\boldsymbol{\alpha}_y - \omega_x\omega_y\boldsymbol{\alpha}_x\\ \omega_x\omega_y\boldsymbol{\alpha}_y - \left(\omega_z^2+\omega_x^2\right)\boldsymbol{\alpha}_x\\ \omega_z\omega_x\boldsymbol{\alpha}_y - \omega_y\omega_z\boldsymbol{\alpha}_x\end{bmatrix}$$

As for $\boldsymbol{\Phi}$, as shown in the equation at the top of the next page.

Hence, we can express $\mathbf{H}\boldsymbol{\Phi}$ from the observability matrix as follows.

$$\mathbf{H}\boldsymbol{\Phi} = \begin{bmatrix}\mathbf{C}_{1,2c} & \boldsymbol{v}_7 & \boldsymbol{v}_8 & \boldsymbol{v}_9 & \boldsymbol{v}_4 & \boldsymbol{v}_5 & \boldsymbol{v}_6\end{bmatrix}$$

where

$$\begin{aligned}
&\boldsymbol{v}_7\\
&= \begin{bmatrix}\mathbf{C}_n^b(1,2)\,g\cdot\mathbf{C}_n^b(1,1)\,\Delta t - \mathbf{C}_n^b(1,1)\,g\cdot\mathbf{C}_n^b(2,1)\,\Delta t\\ \mathbf{C}_n^b(2,2)\,g\cdot\mathbf{C}_n^b(1,1)\,\Delta t - \mathbf{C}_n^b(2,1)^2\,g\cdot\mathbf{C}_n^b(2,1)\,\Delta t\\ \mathbf{C}_n^b(3,2)\,g\cdot\mathbf{C}_n^b(1,1)\,\Delta t - \mathbf{C}_n^b(3,1)\,g\cdot\mathbf{C}_n^b(2,1)\,\Delta t\end{bmatrix}
\end{aligned}$$

$$
\begin{aligned}
\boldsymbol{\Phi} &= \mathbf{I}_{8\times 8} + \mathbf{F}\Delta t \\
&= \mathbf{I}_{8\times 8} + \begin{bmatrix} \mathbf{0}_{2\times 2} & \begin{matrix} \mathbf{C}_n^b(1,1) & \mathbf{C}_n^b(1,2) & \mathbf{C}_n^b(1,3) \\ \mathbf{C}_n^b(2,1) & \mathbf{C}_n^b(2,2) & \mathbf{C}_n^b(2,3) \end{matrix} & \mathbf{0}_{2\times 3} \\ \mathbf{0}_{6\times 2} & \mathbf{0}_{6\times 3} & \mathbf{0}_{6\times 3} \end{bmatrix} \Delta t \\
&= \begin{bmatrix} 1 & 0 & \mathbf{C}_n^b(1,1)\,\Delta t & \mathbf{C}_n^b(1,2)\,\Delta t & \mathbf{C}_n^b(1,3)\,\Delta t & 0 & 0 & 0 \\ 0 & 1 & \mathbf{C}_n^b(2,1)\,\Delta t & \mathbf{C}_n^b(2,2)\,\Delta t & \mathbf{C}_n^b(2,3)\,\Delta t & 0 & 0 & 0 \\ 0 & 0 & 1 & 0 & 0 & 0 & 0 & 0 \\ 0 & 0 & 0 & 1 & 0 & 0 & 0 & 0 \\ 0 & 0 & 0 & 0 & 1 & 0 & 0 & 0 \\ 0 & 0 & 0 & 0 & 0 & 1 & 0 & 0 \\ 0 & 0 & 0 & 0 & 0 & 0 & 1 & 0 \\ 0 & 0 & 0 & 0 & 0 & 0 & 0 & 1 \end{bmatrix}
\end{aligned}
$$

$$
\boldsymbol{v}_8 = \begin{bmatrix} \mathbf{C}_n^b(1,2)\, g \cdot \mathbf{C}_n^b(1,2)\,\Delta t - \mathbf{C}_n^b(1,1)\, g \cdot \mathbf{C}_n^b(2,2)\,\Delta t \\ \mathbf{C}_n^b(2,2)\, g \cdot \mathbf{C}_n^b(1,2)\,\Delta t - \mathbf{C}_n^b(2,1)\, g \cdot \mathbf{C}_n^b(2,2)\,\Delta t \\ \mathbf{C}_n^b(3,2)\, g \cdot \mathbf{C}_n^b(1,2)\,\Delta t - \mathbf{C}_n^b(3,1)\, g \cdot \mathbf{C}_n^b(2,2)\,\Delta t \end{bmatrix}
$$

$$
\boldsymbol{v}_9 = \begin{bmatrix} \mathbf{C}_n^b(1,2)\, g \cdot \mathbf{C}_n^b(1,3)\,\Delta t - \mathbf{C}_n^b(1,1)\, g \cdot \mathbf{C}_n^b(2,3)\,\Delta t \\ \mathbf{C}_n^b(2,2)\, g \cdot \mathbf{C}_n^b(1,3)\,\Delta t - \mathbf{C}_n^b(2,1)\, g \cdot \mathbf{C}_n^b(2,3)\,\Delta t \\ \mathbf{C}_n^b(3,2)\, g \cdot \mathbf{C}_n^b(1,3)\,\Delta t - \mathbf{C}_n^b(3,1)\, g \cdot \mathbf{C}_n^b(2,3)\,\Delta t \end{bmatrix}
$$

To give an example of an unobservable case, we assume a rotation purely about the z-axis. In this case, $\boldsymbol{\omega}_x$, $\boldsymbol{\omega}_y$, $\boldsymbol{\alpha}_x$, and $\boldsymbol{\alpha}_y$ are all zeros. This makes $\boldsymbol{v}_6$, the last column of $\mathbf{H}\boldsymbol{\Phi}$, a null vector, hence indicating that $\delta \mathrm{r}_z$ is unobservable.

REFERENCES

[1] A. Makni, H. Fourati, and A. Y. Kibangou, "Energy-aware adaptive attitude estimation under external acceleration for pedestrian navigation," *IEEE/ASME Trans. Mechatronics*, vol. 21, no. 3, pp. 1366–1375, Jun. 2016, doi: 10.1109/TMECH.2015.2509783.

[2] D. Roetenberg, H. Luinge, and P. Slycke, "Xsens MVN: Full 6DOF human motion tracking using miniature inertial sensors," Xsens Technol. BV, Enschede, The Netherlands, Tech. Rep., Apr. 2013, pp. 1–7, vol. 1.

[3] C. Kim, T. Kim, and J. Lyou, "Realization of a MEMS attitude reference system for a small aerial vehicle," in *Proc. 38th Annu. Conf. IEEE Ind. Electron. Soc.*, Oct. 2012, pp. 1567–1570, doi: 10.1109/IECON.2012.6388507.

[4] S. P. Tseng, W. L. Li, C. Y. Sheng, J. W. Hsu, and C. S. Chen, "Motion and attitude estimation using inertial measurements with complementary filter," in *Proc. IEEE ASCC*, May 2011, pp. 863–868.

[5] R. Mahony, T. Hamel, and J.-M. Pflimlin, "Nonlinear complementary filters on the special orthogonal group," *IEEE Trans. Autom. Control*, vol. 53, no. 5, pp. 1203–1218, Jun. 2008, doi: 10.1109/TAC.2008.923738.

[6] S. Q. Liu and R. Zhu, "A complementary filter based on multi-sample rotation vector for attitude estimation," *IEEE Sensors J.*, vol. 18, no. 16, pp. 6686–6692, Aug. 2018, doi: 10.1109/JSEN.2018.2850943.

[7] J. Wu, Z. Zhou, J. Chen, H. Fourati, and R. Li, "Fast complementary filter for attitude estimation using low-cost MARG sensors," *IEEE Sensors J.*, vol. 16, no. 18, pp. 6997–7007, Sep. 2016, doi: 10.1109/JSEN.2016.2589660.

[8] R. Valenti, I. Dryanovski, and J. Xiao, "Keeping a good attitude: A quaternion-based orientation filter for IMUs and MARGs," *Sensors*, vol. 15, no. 8, pp. 19302–19330, Aug. 2015, doi: 10.3390/s150819302.

[9] R. Kottath, P. Narkhede, V. Kumar, V. Karar, and S. Poddar, "Multiple model adaptive complementary filter for attitude estimation," *Aerosp. Sci. Technol.*, vol. 69, pp. 574–581, Oct. 2017, doi: 10.1016/j.ast.2017.07.011.

[10] E. Vertzberger and I. Klein, "Attitude adaptive estimation with smartphone classification for pedestrian navigation," *IEEE Sensors J.*, vol. 21, no. 7, pp. 9341–9348, Apr. 2021, doi: 10.1109/JSEN.2021.3053843.

[11] M. A. Javed, M. Tahir, and K. Ali, "Cascaded Kalman filtering-based attitude and gyro bias estimation with efficient compensation of external accelerations," *IEEE Access*, vol. 8, pp. 50022–50035, 2020, doi: 10.1109/ACCESS.2020.2980016.

[12] Z. Dai and L. Jing, "Lightweight extended Kalman filter for MARG sensors attitude estimation," *IEEE Sensors J.*, vol. 21, no. 13, pp. 14749–14758, Jul. 2021, doi: 10.1109/JSEN.2021.3072887.

[13] L. Wang, Z. Zhang, and P. Sun, "Quaternion-based Kalman filter for AHRS using an adaptive-step gradient descent algorithm," *Int. J. Adv. Robotic Syst.*, vol. 12, no. 9, p. 131, Sep. 2015, doi: 10.5772/61313.

[14] W. Li and J. Wang, "Effective adaptive Kalman filter for MEMS-IMU/magnetometers integrated attitude and heading reference systems," *J. Navigat.*, vol. 66, no. 1, pp. 99–113, Jan. 2013, doi: 10.1017/S0373463312000331.

[15] R. Munguía and A. Grau, "A practical method for implementing an attitude and heading reference system," *Int. J. Adv. Robotic Syst.*, vol. 11, no. 4, p. 62, Apr. 2014, doi: 10.5772/58463.

[16] X. Tong, Z. Li, G. Han, N. Liu, Y. Su, J. Ning, and F. Yang, "Adaptive EKF based on HMM recognizer for attitude estimation using MEMS MARG sensors," *IEEE Sensors J.*, vol. 18, no. 8, pp. 3299–3310, Apr. 2018, doi: 10.1109/JSEN.2017.2787578.

[17] M.-S. Roh and B.-S. Kang, "Dynamic accuracy improvement of a MEMS AHRS for small UAVs," *Int. J. Precis. Eng. Manuf.*, vol. 19, no. 10, pp. 1457–1466, Oct. 2018, doi: 10.1007/s12541-018-0172-2.

[18] H. Hyyti and A. Visala, "A DCM based attitude estimation algorithm for low-cost MEMS IMUs," *Int. J. Navigat. Observ.*, vol. 2015, pp. 1–18, Nov. 2015, doi: 10.1155/2015/503814.

[19] C. W. Kang, H. J. Kim, and C. G. Park, "A human motion tracking algorithm using adaptive EKF based on Markov chain," *IEEE Sensors J.*, vol. 16, no. 24, pp. 8953–8962, Dec. 2016, doi: 10.1109/JSEN.2016.2607223.

[20] S. M. Esmaeilzadeh, M. Golestani, and S. Mobayen, "Chattering-free fault-tolerant attitude control with fast fixed-time convergence for flexible spacecraft," *Int. J. Control, Autom. Syst.*, vol. 19, no. 2, pp. 767–776, Sep. 2020, doi: 10.1007/s12555-020-0043-3.

[21] Y. S. Suh, "Orientation estimation using a quaternion-based indirect Kalman filter with adaptive estimation of external acceleration," *IEEE Trans. Instrum. Meas.*, vol. 59, no. 12, pp. 3296–3305, Dec. 2010, doi: 10.1109/TIM.2010.2047157.

[22] M. Labbadi and M. Cherkaoui, "Robust adaptive global time-varying sliding-mode control for finite-time tracker design of quadrotor drone subjected to Gaussian random parametric uncertainties and disturbances," *Int. J. Control, Autom. Syst.*, vol. 19, no. 6, pp. 2213–2223, Mar. 2021, doi: 10.1007/s12555-020-0329-5.

[23] A. M. Sabatini, "Quaternion-based extended Kalman filter for determining orientation by inertial and magnetic sensing," *IEEE Trans. Biomed. Eng.*, vol. 53, no. 7, pp. 1346–1356, Jul. 2006, doi: 10.1109/TBME.2006.875664.

[24] J. K. Lee, E. J. Park, and S. N. Robinovitch, "Estimation of attitude and external acceleration using inertial sensor measurement during various dynamic conditions," *IEEE Trans. Instrum. Meas.*, vol. 61, no. 8, pp. 2262–2273, Aug. 2012, doi: 10.1109/TIM.2012.2187245.
[25] M. T. Sabet, H. Mohammadi Daniali, A. Fathi, and E. Alizadeh, "A low-cost dead reckoning navigation system for an AUV using a robust AHRS: Design and experimental analysis," *IEEE J. Ocean. Eng.*, vol. 43, no. 4, pp. 927–939, Oct. 2018, doi: 10.1109/JOE.2017.2769838.
[26] H. Ahmed and M. Tahir, "Accurate attitude estimation of a moving land vehicle using low-cost MEMS IMU sensors," *IEEE Trans. Intell. Transp. Syst.*, vol. 18, no. 7, pp. 1723–1739, Jul. 2017, doi: 10.1109/TITS.2016.2627536.
[27] J. Lee and M. Choi, "Robust inertial measurement unit-based attitude determination Kalman filter for kinematically constrained links," *Sensors*, vol. 19, no. 4, p. 768, Feb. 2019, doi: 10.3390/s19040768.
[28] P. Malinák, M. Soták, Z. Kana, R. Baránek, and J. Duník, "Pure-inertial AHRS with adaptive elimination of non-gravitational vehicle acceleration," in *Proc. IEEE/ION Position, Location Navigat. Symp. (PLANS)*, Apr. 2018, pp. 696–707, doi: 10.1109/PLANS.2018.8373445.
[29] S. Park, J. Park, and C. G. Park, "Adaptive attitude estimation for low-cost MEMS IMU using ellipsoidal method," *IEEE Trans. Instrum. Meas.*, vol. 69, no. 9, pp. 7082–7091, Sep. 2020, doi: 10.1109/TIM.2020.2974135.
[30] S. O. H. Madgwick, A. J. L. Harrison, and R. Vaidyanathan, "Estimation of IMU and MARG orientation using a gradient descent algorithm," in *Proc. IEEE Int. Conf. Rehabil. Robot.*, Jun. 2011, pp. 1–7, doi: 10.1109/ICORR.2011.5975346.
[31] X. Ning and L. Liu, "A two-mode INS/CNS navigation method for lunar rovers," *IEEE Trans. Instrum. Meas.*, vol. 63, no. 9, pp. 2170–2179, Sep. 2014, doi: 10.1109/TIM.2014.2307972.
[32] M. Yu, "INS/GPS integration system using adaptive filter for estimating measurement noise variance," *IEEE Trans. Aerosp. Electron. Syst.*, vol. 48, no. 2, pp. 1786–1792, Apr. 2012, doi: 10.1109/TAES.2012.6178100.
[33] J. F. Wagner, V. Lippens, V. Nagel, M. M. Morlock, and M. Vollmer, "Generalising integrated navigation systems: The example of the attitude reference system for an ankle exercise board," in *Proc. Symp. Gyro Tech.*, Sep. 2001, p. 18.
[34] I. Skog, P. Handel, J. O. Nilsson, and J. Rantakokko, "Zero-velocity detection—An algorithm evaluation," *IEEE Trans. Biomed. Eng.*, vol. 57, no. 11, pp. 2657–2666, Nov. 2010, doi: 10.1109/TBME.2010.2060723.
[35] R. Takeda, S. Tadano, A. Natorigawa, M. Todoh, and S. Yoshinari, "Gait posture estimation using wearable acceleration and gyro sensors," *J. Biomechanics*, vol. 42, no. 15, pp. 2486–2494, Nov. 2009, doi: 10.1016/j.jbiomech.2009.07.016.
[36] D. Laidig, M. Caruso, A. Cereatti, and T. Seel, "BROAD—A benchmark for robust inertial orientation estimation," *Data*, vol. 6, no. 7, p. 72, Jun. 2021, doi: 10.3390/data6070072.
[37] V. Madyastha, V. Ravindra, S. Mallikarjunan, and A. Goyal, "Extended Kalman filter vs. error state Kalman filter for aircraft attitude estimation," in *Proc. AIAA Guid., Navigat., Control Conf.*, Aug. 2011, pp. 6615–6637.
[38] P. G. Savage, "Strapdown inertial navigation integration algorithm design part 1: Attitude algorithms," *J. Guid., Control, Dyn.*, vol. 21, no. 1, pp. 19–28, Jan. 1998, doi: 10.2514/2.4228.
[39] D. Simon, "The discrete-time Kalman filter," in *Optimal State Estimation*, 1st ed. Hoboken, NJ, USA: Wiley-Interscience, 2006, ch. 5, pp. 123–148.
[40] J. F. Wagner, M. Kohl, and B. Györfi, "Reevaluation of algorithmic basics for ZUPT-based pedestrian navigation," *IEEE Access*, vol. 10, pp. 118419–118437, 2022, doi: 10.1109/ACCESS.2022.3220629.
[41] D. Goshen-Meskin and I. Y. Bar-Itzhack, "Observability analysis of piecewise constant systems. II. Application to inertial navigation in-flight alignment (military applications)," *IEEE Trans. Aerosp. Electron. Syst.*, vol. 28, no. 4, pp. 1068–1075, Oct. 1992, doi: 10.1109/7.165368.
[42] *MTi and MTx User Manual and Technical Documentation*, Xsens Technol. BV, Enschede, The Netherlands, 2009, pp. 16–17.

MIN SEOK LEE (Graduate Student Member, IEEE) received the B.S. degree in mechanical and aerospace engineering from Seoul National University, Seoul, South Korea, in 2021, where he is currently pursuing the M.S. degree in aerospace engineering. His current research interests include attitude reference systems and visual-inertial odometry.

JUNGMIN PARK received the B.S. degree in physics education and aerospace engineering and the M.S. degree in aerospace engineering from Seoul National University, Seoul, South Korea, in 2017 and 2019, respectively. She is currently with the Agency for Defense Development, Daejeon, South Korea. Her research interests include navigation and filtering techniques.

CHAN GOOK PARK (Member, IEEE) received the B.S., M.S., and Ph.D. degrees in control and instrumentation engineering from Seoul National University, Seoul, South Korea, in 1985, 1987, and 1993, respectively. He was a Postdoctoral Fellow with Prof. Jason L. Speyer about Peak Seeking Control for Formation Flight with the University of California at Los Angeles, Los Angeles, CA, USA, in 1998. From 1994 to 2003, he was an Associate Professor with Kwangwoon University, Seoul. In 2003, he joined the Faculty with the School of Mechanical and Aerospace Engineering, Seoul National University, where he is currently a Professor. In 2009, he was a Visiting Scholar with the Department of Aerospace Engineering, Georgia Institute of Technology, Atlanta, GA, USA. His current research interests include advanced filtering techniques, high-precision inertial navigation systems (INSs), visual-inertial odometry (VIO), INS/GNSS/IGN integration, and smartphone-based/foot-mounted pedestrian dead reckoning (PDR) systems. He served as the Chair for IEEE AES Korea Chapter until 2009.